NTIA REPORT 81-76

Electromagnetic Compatibility Analysis for a Satellite Power System Receiving Site in the Mojave Desert

E.L. Morrison
W.B. Grant
E.J. Dutton

U.S. DEPARTMENT OF COMMERCE
Malcolm Baldrige, Secretary

Bernard J. Wunder, Jr., Assistant Secretary
for Communications and Information

June 1981

TABLE OF CONTENTS

LIST OF FIGURES

LIST OF TABLES

ELECTROMAGNETIC COMPATIBILITY ANALYSIS FOR A SATELLITE POWER SYSTEM RECEIVING SITE IN THE MOJAVE DESERT

E. L. Morrison, W. B. Grant, and E. J. Dutton*

The Department of Energy (DOE), along with the National Aeronautics and Space Administration (NASA), has been evaluating the Satellite Power System (SPS) as a source of baseline electrical power. The objective of the SPS program is to develop an initial understanding of the technical feasibility, the economic practicality, and the social and environmental acceptability of the SPS concept. One of the potential problems identified early in the concept analysis was the electromagnetic compatibility (EMC) of an SPS with existing and planned electromagnetic and electronic systems. A preliminary study has been conducted to show the EMC problems for an initial candidate receiving antenna (rectenna) site in the Mojave Desert of California. A methodology has been developed and demonstrated for rectenna site EMC analysis and impact evaluation. For the particular site chosen, the majority of the severe impact interference problems concerned military operations. The systems degraded by SPS off-site microwave beam components were integral systems and subsystems of complex Development and Operational Test and Evaluation programs. Based on the operational system degradations near the Mojave site and the inability to establish mitigating strategies without unacceptable operational compromise, a second site north and east of the original was proposed.

1. INTRODUCTION

The Department of Energy (DOE), in the pursuit of developing new energy sources, has been actively studying Solar Power System (SPS) concepts in conjunction with NASA. One concept under study would convert the sun's energy to direct-current electrical energy using large collector panels on a geostationary satellite. This dc energy would then drive high-power microwave devices on board the satellite to produce a high-energy microwave beam aimed at a receiving antenna (rectenna) on earth, where it would be converted to dc energy for use in the electrical power distribution system. One satellite is to be capable of producing 5000 megawatts of power at the rectenna.

There has been a continuous concern that the high-energy microwave beam presents an electromagnetic compatability (EMC) problem with existing communication, radar, and other electronic systems that could be illuminated by a component of the SPS power beam. In this study, the potential EMC problems were assessed for an initial hypothetical rectenna site in the Mojave Desert of California.

---

*The authors are with the U.S. Department of Commerce, National Telecommunications and Information Administration, Institute for Telecommunication Sciences, Boulder, Colorado 80303.

The EMC susceptibility of systems has been generally site independent; the study identifies critical illumination levels outside the rectenna exclusion zone and identifies potential EMC problems for general classes of equipment. The Mojave exercise demonstrated the basic methodology to be used to assess EMC problems in support of rectenna siting criteria development and, ultimately, candidate site selection. This included identification of system functional degradation due to SPS illumination and mitigation techniques prioritized according to degree of effectiveness versus cost.

2. SCOPE

The following are within the scope of this report:

Characterization of the EM environment surrounding a rectenna site from main beam sidelobes and media scattered components.

An assessment of the electromagnetic compatibility (EMC) of SPS with EM receiver systems.

Analysis of the implications in the vicinity of the Mojave site of the induced degradation because of SPS illumination.

3. METHODOLOGY

3.1 EMC Analysis and Evaluation

The potential EMC problem caused by the satellite power systems is recognized as one of the most critical in the SPS environmental assessment. Consequently, an aggressive program has been initiated to perform analysis of the functional and operational degradation of electromagnetically sensitive systems (e.g., communication, radar, navigational, computer, sensors, electronic medical instruments and devices, etc.) because of SPS direct power coupling and ionosphere and atmosphere media modification effects. These effects are pictorially shown in Figure 3.1. Primary evaluation areas include EM environment verification computations, SPS energy coupling analysis, functional-operational degradation evaluations of the sensitive systems listed above, priority categorization, and impact assessment. Subsequent tasks address mitigation methods for degraded systems and guidelines for designers and planners of future systems.

The SPS system parameters and characteristics derived, based on the reference design, include: single satellite microwave power transmission system radiation characteristics, fundamental emission power spectra, sidelobe structure, and estimates of harmonic power outputs. A model was implemented to predict field strengths at and near the surface of the earth from SPS microwave emissions. An

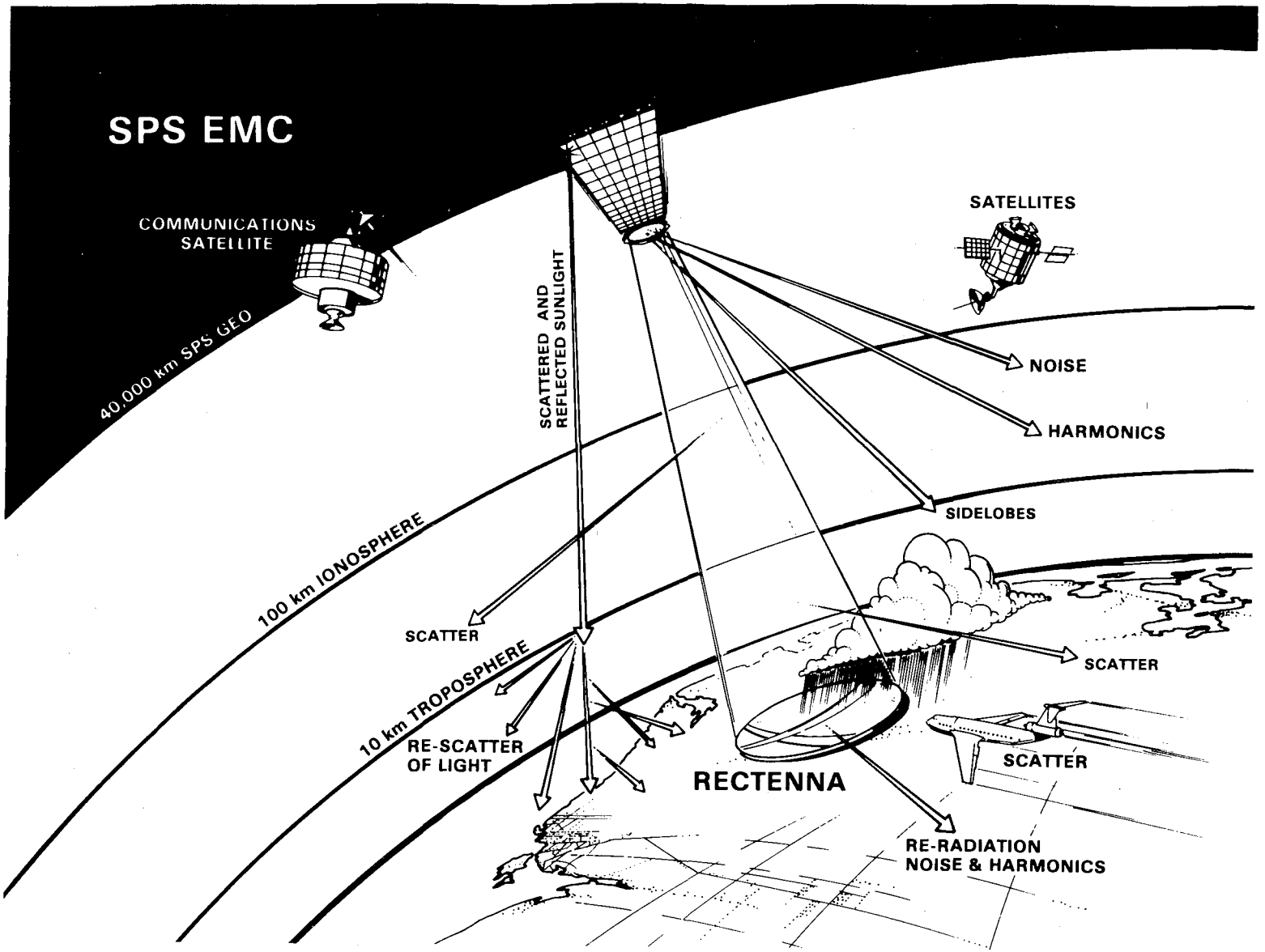

Figure 3.1. EMC considerations for an SPS.

analysis was accomplished to determine EM energy scattered from the main beam by atmospheric phenomena to help characterize the EM environment in close proximity to a rectenna site. Equipments and systems near the rectenna site susceptible to SPS radiation are identified by selective retrieval from existing files and categorized in relation to function, coupling modes, location, and interconnectivity. Functional degradation as a result of the SPS interference magnitudes include all performance events required to define supported operational compromises. Signal-to-interference ratios (S/I) representing scoring models were designed to be multidimensional to allow adequate definition of the operational relationships. These are demonstrated in the functional degradation summaries presented in Table 7.1. Signal/interference scoring models were designed for victim systems (those systems affected by SPS illumination), and confirmatory signal-SPS interference ratio tests were conducted on candidate systems where data voids existed.

Subsequent to the degradation analyses, modification techniques applicable to affected Continental U.S. (CONUS) systems are being evaluated to allow an acceptable operational capability for electronic equipments within the SPS environment. Implementation procedures and cost estimates, including priorities, are being developed.

3.2 Cause-Effects Relationships

Cause and effect relationships are summarized graphically in Fig. 3.2. These indicate the atmospheric media effects on the SPS power and pilot beams, and the energy coupling to a number of electronic systems. Before an EMC analysis of any given site can be performed, the EM environment surrounding that site must be characterized identifying total potential fields generated by an SPS.

Various atmospheric parametric interactions affect the power efficiency of the SPS system and increase the interference problem because of power-beam refraction and scatter. These are:

attenuation because of atmospheric gases and stratification;
attenuation and scatter due to precipitation, - rain, hail, etc.;
attenuation and scatter due to dust and other particulates; and
wavefront distortions due to turbulence with or without accompanying stratification.

These properties of the atmosphere vary seasonally, diurnally, and with geographic location.

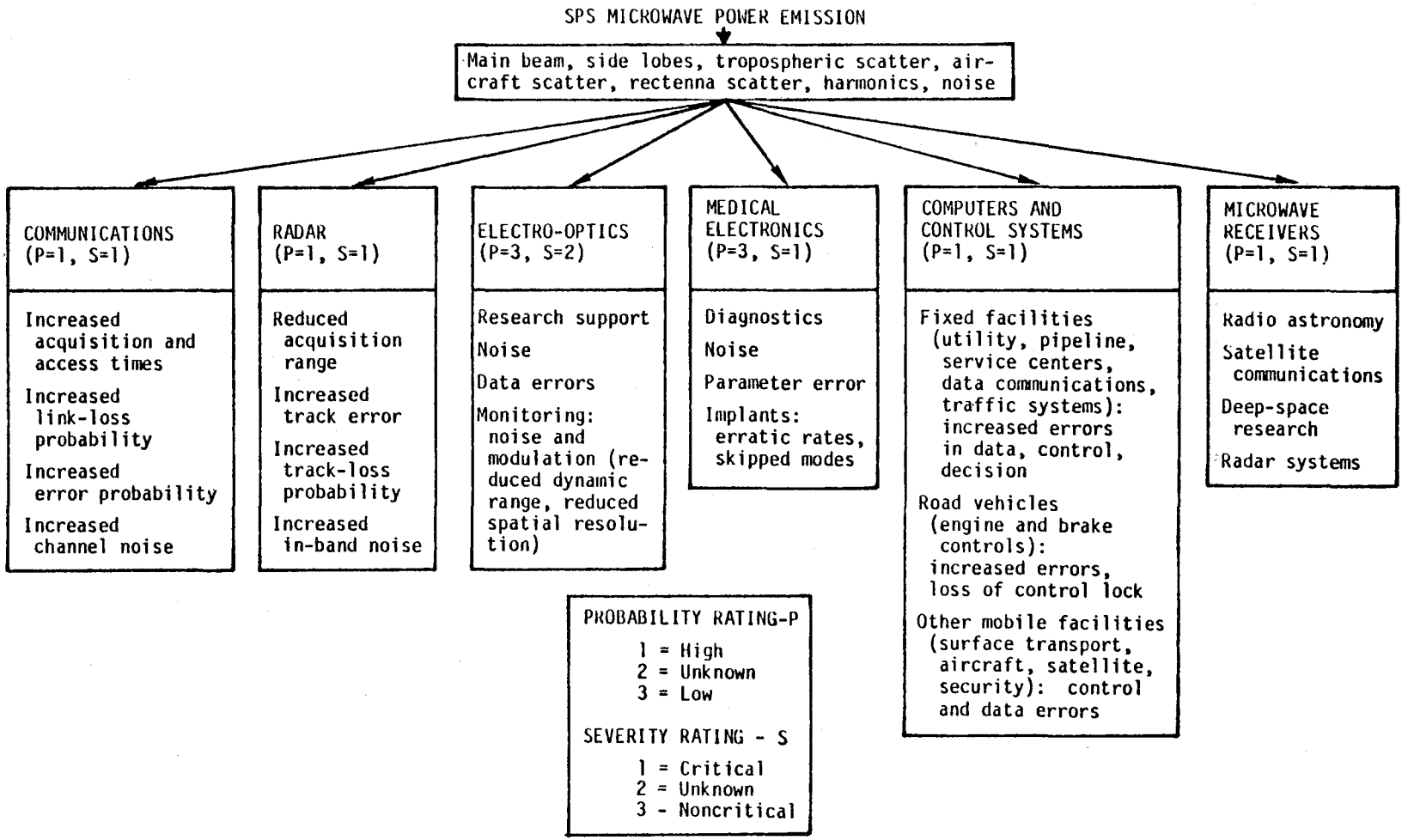

Figure 3.2. Effects of SPS microwave transmission on electromagnetically-sensitive systems.

Atmosphere media effects are of two general types: long-term variations extending over a time scale of "hours" and short-term "transients" such as angels (drifting atmosphere refractive index anomalies) and turbulence, particulate and precipitation scatter during storms, and passing storm fronts.

These various media effects also represent different power-beam control response problems. Media effect magnitudes and the detection and processing of power-beam parameters to extract atmosphere "signatures" must be carefully addressed in the pilot beam-array control loop design to positively minimize ambiguities, instability probabilities, and aiming errors due to these media effects. These areas have important implications for future modular and subsystem laboratory testing.

Attenuation and scattering due to precipitation and anomaly refraction also cause power level fluctuations as received at the rectenna. This is generally proportional to rain rate and anomaly density. The effect is directly analogous to the aperture modulation functions that can degrade target identification and tracking capabilities for phased array radars. Blowing dust or sand contributes to a lesser degree to beam-power attenuation and scattering of energy. Although each mechanism alone would have seemingly small effects stated as a percentage of main beam power or in decibel power loss, because of the large power levels involved with SPS, the magnitude of power fluctuations due to these mechanisms may be unacceptable to the distribution system.

The pilot beam required for frequency/phase reference and orbital antenna spatial control is also affected by these same atmospheric mechanisms. Any of these mechanisms discussed under circumstances such as very heavy rain, severe sand storms, etc. could readily induce control loop errors and instabilities resulting in power-beam jitter or wander and frequency fluctuations, which in turn adversely affect power transfer efficiency and exaggerate the interference problems.

The above discussion addressed those mechanisms that would cause modulation of received power at the rectenna and pilot carrier. A related major area of concern is the SPS interference with other electronic systems. If no ionospheric or atmospheric effects were present, there would still be impact outside the rectenna area due to the power-beam sidelobes, emission of harmonics of the primary frequency and spurious components, noise sidebands, and terrain reflections. The SPS emissions from these sources will cover the hemisphere; however, most of the EMC problems will occur within 100 km radius of the rectenna, where the power densities are highest. Radio astronomy and deep space communications terminals

represent interference susceptibility problems at much greater distances from rectenna sites because of the receiver sensitivities and operating bandwidths.

Energy coupling to victim systems involves in-channel and nonlinear responses by out of band components relative to the primary receiver pass band, and coupling through cabling and circuit element apertures to other electronic circuitry. Different performance descriptors scoring is required for rf receivers and sensors or computers because of coupling mode variations and performance criteria. Scoring procedures applicable to this problem can be derived by extrapolation of existing empirical and analytical degradation models for receiver systems employed for communications, radar, or a general range of metering applications. These define a range of performance characteristics in terms of probability density functions for signal-to-interference ratios. Most of the EMC problems related to the SPS that represent a significant expenditure in victim rf receiver modification will be concerned with the nonlinear response category.

Computer devices, optical equipment, and medical instrumentation present unique scoring descriptives that relate to physical apertures and energy coupling into signal and control circuitry and noise conducted through control and "quality" ground circuits from external devices or busses. These types of problems can, to a lesser degree, be extrapolated from experience with high-power radar illumination of surveillance and monitoring equipment required for military operations. Limited measurements will be required for the SPS interference problem to assure credibility in the predicted degradation and recommended functional modifications for these classes of equipment.

Additional EMC related problems that are being addressed at present concern the infrared (IR) source and optical reflection characteristics of the SPS vehicle in temporary and permanent orbit locations. Functional impacts are anticipated for astronomy and space tracking/monitoring equipment because of the probable magnitudes of the emissions and reflections from the large orbiting platform.

3.3 State of Knowledge

In general, the systems most vulnerable to SPS emissions are those that operate in the vicinity of the main beam frequency and harmonics. These are listed.

Primary Frequency	2.45 GHz
2nd harmonic	4.9 GHz
3rd harmonic	7.35 GHz
4th harmonic	9.8 GHz

Included in the band from 2.29 to 2.45 GHz are allocations to radio location and to space research. The radio location assignments have fairly strict requirements as far as radio interference is concerned. The amount of energy from SPS, possibly as far out as 100 km from the rectenna site, may exceed these requirements. The space research assignments are used for telemetry from missile tests, the space shuttle, space platform, and other space related tests. These are particularly vulnerable to SPS emissions because of high-gain directive antennas that will be looking skyward. Receiver sensitivity and bandwidth considerations indicate unacceptable "noise" effects for the space research class of energy receivers within 50 km of a rectenna site. Special filters and shielding could allow operation of these sensitive receivers within about 100 km for the reduced bandwidth instrumentation where the band of interest was at least 100 MHz from the SPS frequency (primary and second harmonic). The interference effects are greater for the radio astronomy band from 2.69 to 2.70 GHz.

From 2.45 to 2.69 GHz, in addition to radio location, there are broadcasting satellite and fixed satellite assignments. Again, sensitive equipment would be vulnerable to SPS emission, particularly for geosynchronous satellites since the terrestrial receiving antennas would be oriented with a sector of the main beam or a principle sidelobe pointed toward the SPS.

From 2.7 to 5 GHz are assignments to aeronautical radio navigation, radio locations, maritime radio navigation, fixed satellite, radio astronomy, meteorological telemetry, and other sensitive systems, which again are subject to severe compatibility problems with SPS. Errors induced by SPS emissions into radio navigation systems range from output errors to loss of track signals because of receiver noise and discrete intermodulation components, depending on the type of system and the distance from SPS main beam. Antenna and circuit modifications are required to allow operation with SPS illumination.

Air-traffic-control communications, radar, and radio navigation aids have very strict interference regulation and standards. Because of safety sensitivities, all interference must be carefully controlled. At frequencies below about 1 GHz and with receivers that are well designed (as are most FAA and aircraft receivers), degradation will not be serious until within 50 km of the rectenna site. Above 1 GHz, additional coupling sensitivities magnify performance degradation.

Surface communications near the rectenna sites will be affected through induced noise and intermodulation components. Performance scores include data

channel noise in demultiplexer operations, increase in data errors, address errors, and sync loss. Surface radars will be affected by increased target acquisition times, increased target lock time, and increased track errors.

Tests have been completed to determine coupling modes and functional affects for a number of minicomputers and modular components. Previous experience with interference problems in minicomputers indicates unacceptable control buss and modular ground methods. Commercial peripheral modules require input-output circuit modifications for illumination levels above 5-10 mw/cm^2.

The medical electronics susceptibility area concerns, primarily, implanted devices, patient telemetry, and remote clinic diagnostic instrumentation. Remote telemetry is expected to operate satisfactorily to SPS illumination levels of about 5 mw/cm^2. Additional cable and modular shielding will be required for diagnostic equipment (EKG, EEG, EMG). For remote clinic applications, patient testing areas should be shielded to accommodate operation in SPS power densities of 0.11 mw/cm^2.

Imaging equipment degradation descriptors have been based on video noise, image detection threshold, dynamic range, and spatial resolution factors. Coupling of rf energy is accomplished through detector (vidicon, semiconductor detector, multiplier tube) apertures and associated control and signal circuitry, usually physically colocated with the detector device. Conductive noise coupling from external transient protector devices and multi-point grounding can also occur for power densities above 0.5 mw/cm^2. Conductive modes are primarily effective with photomultiplier, orthicon, and charge coupled device (CCD) detector configurations.

3.4 Program Methodology

The EMC evaluation program includes the listed elements.

1. Definition of SPS emission characteristics: modulation sidebands, harmonics, spatial patterns, field strength projections surrounding a given site and projected out to a hemisphere.

2. Application of propagation models to develop power density contour variations caused by atmosphere and meteorological anomalies to characterize the EM environment surrounding a rectenna site.

3. Categorization of susceptible electronic equipments, and operations or services supported.

4. Specification of degradation criteria for susceptible equipments/systems. Performance scoring descriptors for related single or multiple functions to SPS interference amplitudes.

5. Analysis and testing of system categories: identifying modes of energy penetration and coupling, and performance effects.

6. Identification of operational support impacts, generally through safety and command/control effectiveness sets of criteria.

7. Specification and testing of mitigation methods to allow equipment/system performance in SPS illumination densities ≤ 1 mw/cm^2 for terrestrial systems, and to allow operation during passage through the main power beam for low-earth-orbit (LEO) satellites.

Scoring criteria and descriptors are presented in Section 5 of this report.

Atmospheric propagation models have been developed to describe frequency dependent characteristics as listed in Table 3.1. The models relating these propagation and atmosphere characteristics are modified to accommodate sensitivity analysis, particularly short-term powerbeam scatter and refraction variations with local area meteorology. For a separate design support application, coherence properties will be provided to describe rectenna power density variations and rectenna area terrain effects. This task involves organizational modification and meteorology parameter relationship definition.

Table 3.1 List of Propagation - Meteorology Parameters

Propagation Parameters	Meteorology Parameters
a. Attenuation	a. Temperature and pressure gradients
b. Rain, hail, particulate scatter	b. Humidity profiles
c. Refractive anomalies	c. Wind profiles
d. Refractive gradients	d. Turbulence properties
e. Terrain reflection	

From considerations of the EMC impact, another alternative in SPS characteristics is being examined: modification of the transmission frequency from the 2.45 GHz principal candidate. Current frequency alternatives all relate to higher bands: 6 GHz through the 33 GHz regions. The EMC advantages primarily accrue in the regions above 10 GHz because of the reduced allocations and specific assignments in the military and civil sectors and the predominant use of narrow beam antennas relative to EM systems in the lower spectral regions.

The SPS system performance would be impacted in varying degrees by operation at these higher frequencies: increased atmosphere attenuation, scatter, and

refractive anomaly sensitivity. General exponential atmosphere parameter relationships prevail, with absorption and transmission windows available at discrete frequencies above 30 GHz. For the power ranges required for SPS, space generation equipment development and operational uncertainties for the regions above 20 GHz limit the detailed design. The general allocation and assignment situation in relation to the higher microwave spectral regions is shown in Figure 3.3. Looking toward the 1990-2010 era, these regions will be approaching "congestion" with the planned satellite and terrestrial communications and sensing operations.

For these higher frequencies, the spacetenna and rectenna would be physically smaller for system functional parameters identical with 2.45 GHz operation. Control and operational stability problems would, however, be aggravated because of the increased atmospheric interactions. The alternate frequency analysis is detailed in a separate technical report.

Higher frequencies would also practically eliminate the possible ionosphere beam distortion and parametric modification effects. Heating and dynamic perturbations would be negligible at frequencies higher than 30 GHz.

Lower frequencies cannot be considered because of the increased victim system densities within CONUS and other developing nations. The increased interference would affect military and civil domains and directly increase the susceptibility of VHF and sensor equipments because of circuit impedance and coupling aperture factors. Lower frequencies also represent higher ionospheric modification.

4. SPS EMISSION CHARACTERISTICS

The SPS interferer is defined by the spectral and spatial emission characteristics. For the EMC evaluation, the fundamental and harmonic amplitude modulation sidebands, spatial patterns for the fundmental and harmonic components, and intermodulation components generated by the driver and output power amplifiers and space vehicle structural member currents are included. For the terrestrial EMC emphasis in the MOJAVE site evaluation, the intermodulation emissions can be omitted since the total power is expected to be $< 10^6$ lower than the fundamental, distributed over the HF to lower UHF spectrum, and radiated nearly constant over a sphere centered at the rectenna. These components must be considered in the evaluation of SPS impacts on low-earth-orbit (LEO) and geosynchronous-orbit (GEO) satellites and high altitude military aircraft.

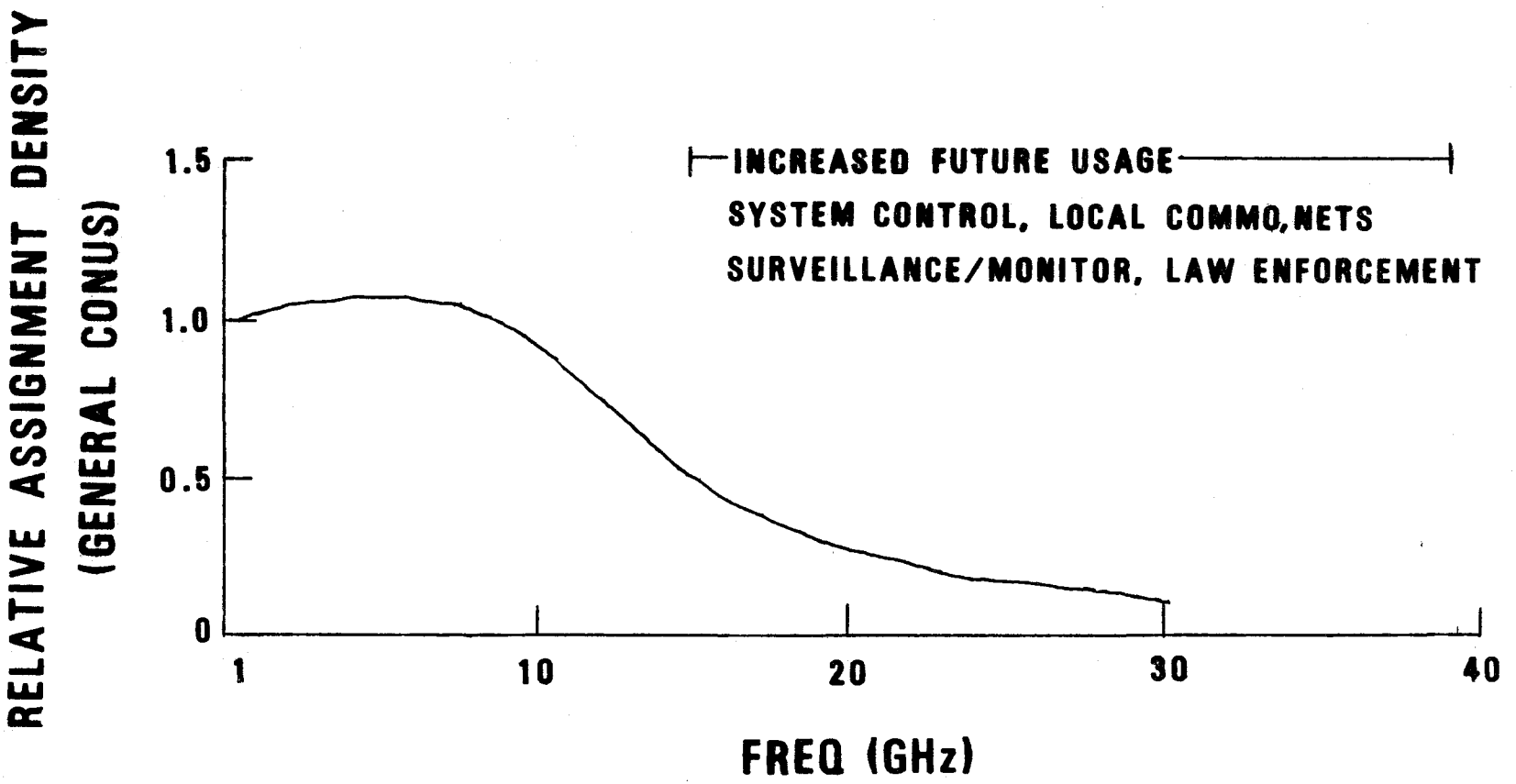

Figure 3.3. General spectrum assignment densities.

The modulation sideband and harmonic amplitudes assumed coupled into the space array are indicated in Figures 4.1 and 4.2. The sideband data representing a current klystron model is indicated, but is considered generally representative of this class of tube and is used here as representative of what emissions from an SPS klystron might be. Harmonic distributions represent a number of klystron amplifiers in the 10 kW to 75 kW range employed for radar applications. These harmonic tests were conducted in CW and pulse modes. A computer program was developed to characterize the fundamental frequency radiation pattern. The radiation pattern of circular apertures is readily derivable when the distribution across the aperture is uniform in amplitude and phase. Born and Wolf (1959) give a clear and correct derivation for the radiation pattern for the case of uniform illumination. This analysis was extended for the case of the amplitude across the aperture defined by a finite number of steps in the radial direction and is circularly symmetric. A computer program was developed to perform the calculations for the radiation pattern of the spacetenna over a complete hemisphere. The spacetenna fundamental frequency pattern derivation near boresight and at other selected angular segments is discussed in the following pages.

Predictions of harmonic spatial patterns are based on extrapolation of spectrum signature data for the SPY1 and COBRA DANE radars. These array systems have dipole elements with $\lambda/2$ spacing, although the diameter-wavelength (D/λ) ratio is reduced by approximately 40 and 10, respectively.

Extrapolating to the D/λ for the spacetenna (8.3×10^3) and applying a 5-point smoothing routine to provide an averaged pattern produces pattern estimates for f_2 and f_3 as plotted in Figures 4.3 and 4.4. These averaged plots provide spatial distribution estimates for the EMC evaluation. The computations for ωf_2 and ωf_3 use 30° pattern segments to provide gain references (zero frequency reference in the spatial frequency domain). A 5-point smoothing routine derives an envelope for the patterns, allowing conservative and much less complex harmonic power density computations for the sensitive electronic system EMC evaluations. These patterns would obviously have no utility in any control study involving sidelobe or energy distribution management procedure specifications, such as minimizing harmonic emission peaking and orthogonal sidelobes in the direction of other GEO SATELLITES. The patterns are only useful to provide an

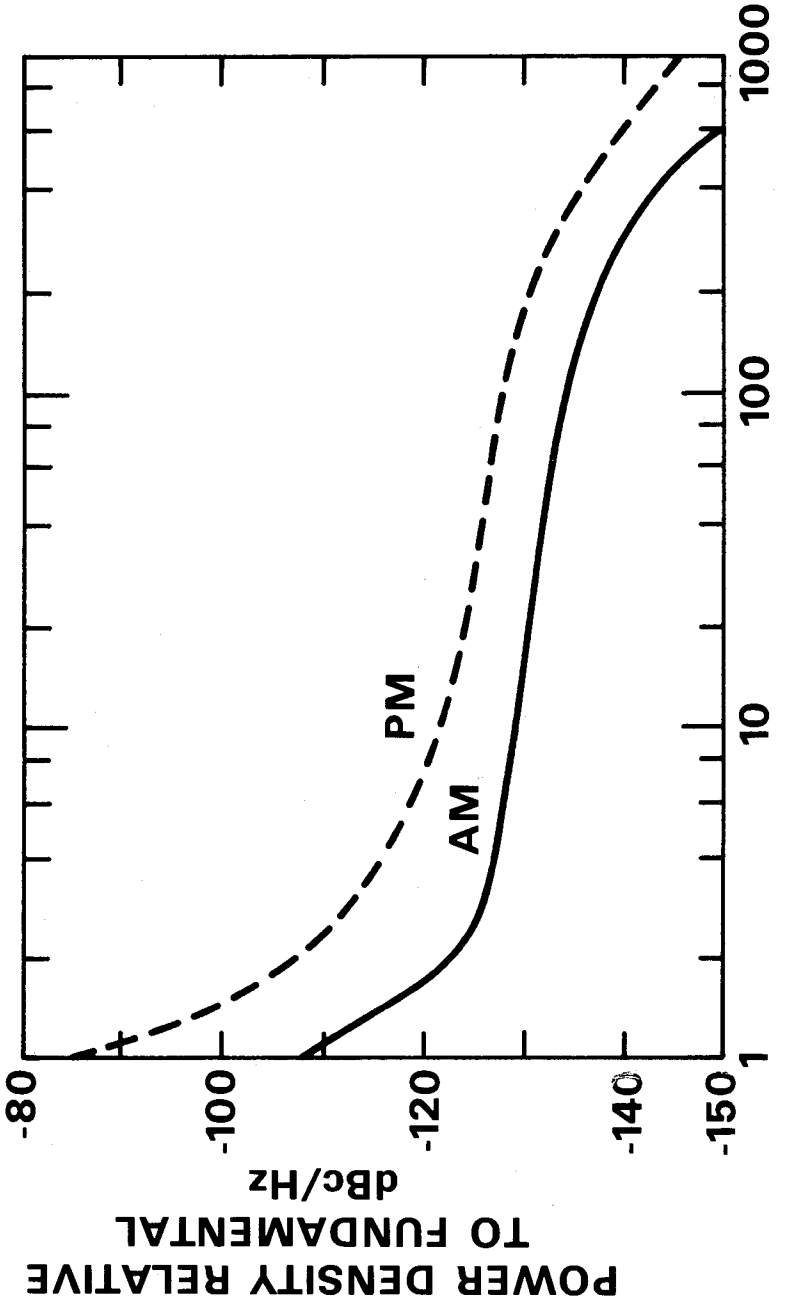

Figure 4.1. Typical noise emissions from a high power klystron.

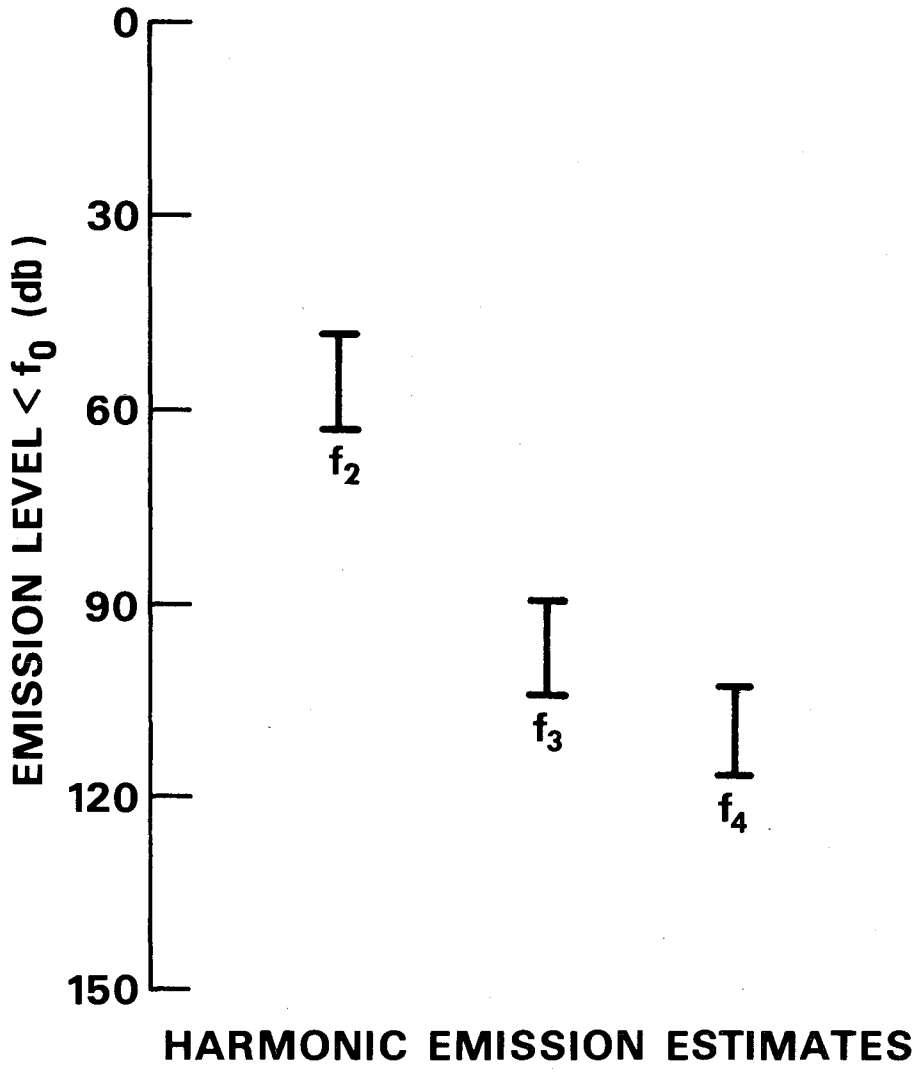

Figure 4.2. Typical harmonic emission from a high power klystron.

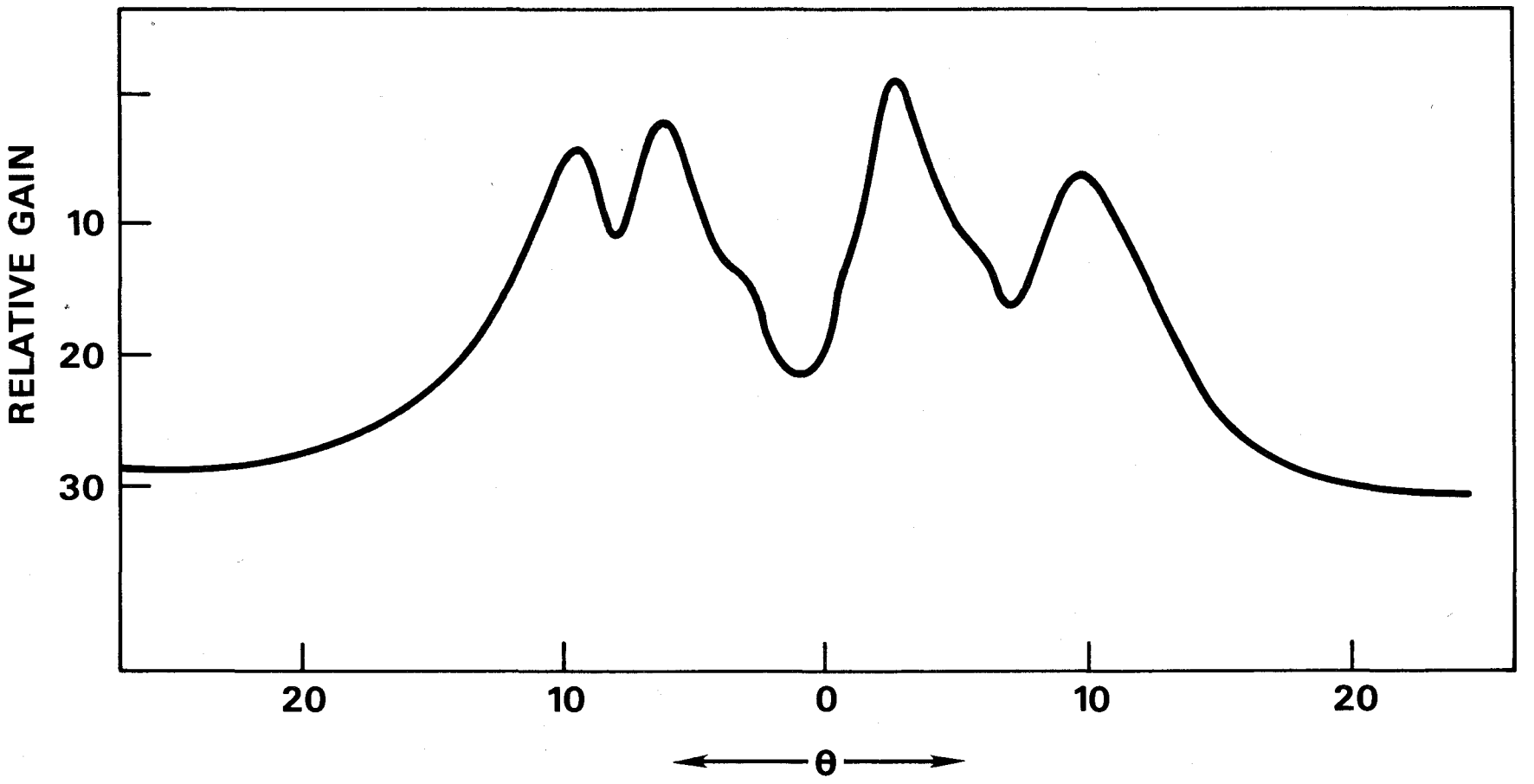

Figure 4.3. Spacetenna - f_2 pattern estimate.

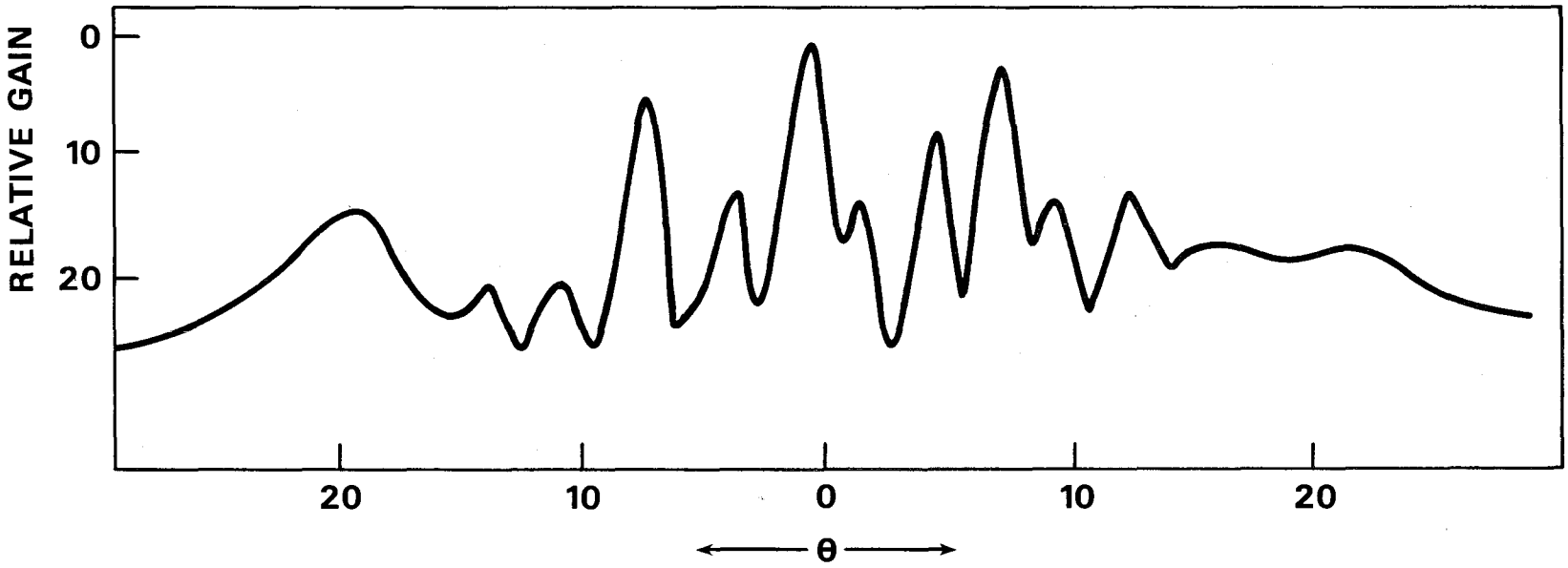

Figure 4.4. Spacetenna - f_3 pattern estimate.

estimate of harmonic power coupling to susceptible electronic systems and the specification of techniques to mitigate power coupling, and provide a specification for harmonic emission limits for the SPS.

Before developing the analysis, we discuss the near-field or Fresnel region for the spacetenna. The $2D^2/\lambda$ criteria suggests the transition from near to far field occurs at a distance of about 1.63×10^4 km from the antenna. A heuristic derivation for the near field gain of the antenna goes as follows: the gain, at any distance from the antenna, is defined as

$$G(\theta,\phi) = \frac{\text{Max. Radiation Intensity}}{\text{Ave. Radiation Intensity}} \quad . \tag{1}$$

The maximum radiation intensity at a distance R from the antenna is $R^2 P_R$, where P_R is the radial component of the average Poynting vector taken in the boresight direction from the antenna. Now

$$\begin{aligned} \text{Ave. Radiation Intensity} &= \frac{1}{4\pi} \int_0^{2\pi} d\phi \int_0^{\pi} \sin\theta d\theta \; P_R(\theta,\phi) \\ &= \frac{1}{4\pi} \text{ total radiated power} \end{aligned} \tag{2}$$

and we approximate the total radiated power by the radial component of the Poynting vector in the boresight direction times the area of the antenna perpendicular to boresight. This yields the minimum radiated power since the radiation pattern covers a complete hemisphere about boresight. We therefore obtain an upper bound for the near field gain as

$$G \leq \frac{R^2 \; P_R}{\frac{1}{4\pi} \text{ area } P_R} = \frac{4\pi R^2}{\text{Area}} = \frac{4\pi}{\pi/4} \left(\frac{R}{d} \right)^2 = 16 \left(\frac{R}{d} \right)^2$$

or

$$G \leq 16 \left(\frac{R}{d} \right)^2 \tag{3}$$

where d = antenna diameter. For the SPS spacetenna, (3) yields G = 76 dB at a distance of 1600 km, which corresponds to a 11.6 dB loss in gain at the specified near-field distance. We show later the on-axis gain is about 87.65 dB, so the above loss reduces the on-axis gain to about 76 dB. In contrast, the radiated power density, P_R, is greater in the near field than far field, being approximately constant with distance from the aperture along the boresight direction for an aperture with uniform illumination (White, 1972). For the constant aperture illumination case, the e.i.r.p. (effective isotropic radiated power), which is the product of the input power in watts times the gain, will decrease with distance according to (3) in the near field.

Returning to the derivation for the gain of the SPS spacetenna, consider the geometry shown in Figure 4.5, where the observer is now assumed to be in the Fraunhofer region. The fields are given by (Born and Wolf, 1959)

$$\begin{Bmatrix} E_\phi \\ E_\theta \end{Bmatrix} = \begin{Bmatrix} (\sin\theta+\cos\phi) \\ -\sin\phi\cos\theta \end{Bmatrix} \frac{ie^{-ikr}}{2\lambda r} \int_0^{2\pi} d\beta' \int_0^a \rho' d\rho' f(\rho',\beta') e^{-ik\rho'\cos\psi}, \quad (4)$$

where $f(\rho', \beta')$ is the field distribution in the aperture, the angle ψ is defined by

$$\cos\psi = \underline{e}_r \cdot \underline{e}_{\rho'} \quad (5)$$

with $\underline{e}_r$ and $\underline{e}_\rho$, unit vectors in the r and ρ' directions, respectively; $k = 2\pi/\lambda$ is the free space wave number with λ the free space wavelength. The unit vectors $\underline{e}_r$ and $\underline{e}_\rho$ are given by

$$\underline{e}_r = \underline{e}_x \cos\alpha + \underline{e}_y \sin\alpha\sin\beta + \underline{e}_z \sin\alpha\cos\beta \quad (6)$$

$$\underline{e}_{\rho'} = \underline{e}_y \sin\beta' + \underline{e}_z \cos\beta' \quad (7)$$

so that

$$\cos\psi = \sin\alpha\cos(\beta - \beta'). \quad (8)$$

Substituting (8) in (4) gives

$$\begin{Bmatrix} E_\phi \\ E_\theta \end{Bmatrix} = \begin{Bmatrix} (\sin\theta+\cos\phi) \\ -\sin\phi\cos\theta \end{Bmatrix} \frac{ie^{-ikr}}{2\lambda r} \int_0^a d\rho' \int_0^{2\pi} d\beta' \rho' f(\rho',\beta') e^{-ik\rho'\sin\alpha\cos(\beta-\beta')}. \tag{9}$$

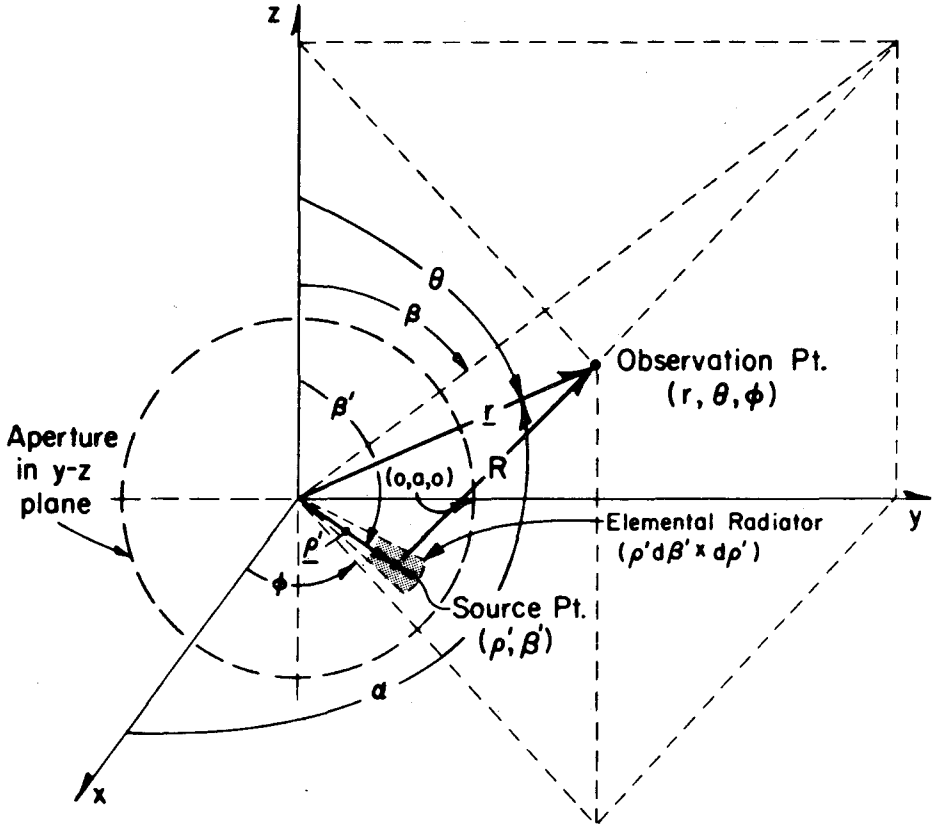

Figure 4.5. Geometry for derivation of radiation pattern.

Now we assume the aperture distribution is given by

$$f(\rho',\beta') = \sum_{j=1}^{N} A_j(\rho') \tag{10}$$

and substituting (10) in (9) yields

$$\begin{Bmatrix} E_\phi \\ E_\theta \end{Bmatrix} = \begin{Bmatrix} (\sin\theta+\cos\theta) \\ -\sin\phi\cos\theta \end{Bmatrix} \frac{ie^{-ikr}}{2\lambda r} \sum_{j=1}^{N} \int_0^a \rho' d\rho' A_j(\rho') \int_0^{2\pi} d\beta' e^{ik\rho'\sin\alpha\cos(\beta-\beta')}. \tag{11}$$

We use the well known definition for Bessel function

$$2\pi\, J_o(k\rho'\sin\alpha) = \int_o^{2\pi} d\beta'\; e^{-ik\rho'\sin\alpha\cos(\beta-\beta')} \tag{12}$$

to obtain

$$\begin{Bmatrix} E_\phi \\ E_\theta \end{Bmatrix} = \begin{Bmatrix} (\sin\theta+\cos\phi) \\ -\sin\phi\cos\theta \end{Bmatrix} \frac{i\pi e^{-ikr}}{\lambda r} \sum_{j=1}^{N} \int_o^a A_j(\rho') J_o(k\rho'\sin\alpha)\rho' d\rho' . \tag{13}$$

Since $A_j(\rho')$ is constant in each step, j,

$$\begin{Bmatrix} E_\phi \\ E_\theta \end{Bmatrix} = \begin{Bmatrix} (\sin\theta+\cos\phi) \\ -\sin\phi\cos\theta \end{Bmatrix} \frac{i\pi e^{-ikr}}{\lambda r} \sum_{j=1}^{N} A_j \int_{\beta_j}^{\beta_{j+1}} J_o(k\rho'\sin\alpha)\rho' d\rho' . \tag{14}$$

Now, we have

$$\int J_o(k\rho'\sin\alpha)\rho' d\rho' = \frac{\rho'}{k\sin\alpha} J_1(k\rho'\sin\alpha) , \tag{15}$$

and substituting (15) into (14) gives

$$\begin{Bmatrix} E_\phi \\ E_\theta \end{Bmatrix} = \begin{Bmatrix} (\sin\theta + \cos\phi) \\ -\sin\phi\cos\theta \end{Bmatrix} \frac{i\, e^{-ikr}}{2r\sin\alpha} \sum_{j=1}^{N} A_j \left[\beta_{j+1} J_1(k\beta_{j+1}\sin\alpha) - \beta_j J_1(k\beta_j\sin\alpha)\right] . \tag{16}$$

Since

$$\cos\alpha = \underline{e}_r \cdot \underline{e}_x = \cos\phi\sin\theta , \tag{17}$$

we find

$$\sin\alpha = \sqrt{1-\cos^2\phi\sin^2\theta} . \tag{18}$$

The radiation intensity is defined as

$$K(\theta,\phi) = \frac{r^2(|E_\theta|^2 + |E_\phi|^2)}{2Z_o} \tag{19}$$

where $Z_o = 377\Omega$ is the impedance of free-space. Substituting (16) and (18) into (19) gives the desired result:

$$K(\theta,\phi) = \left(\frac{1}{8Z_o}\right) \frac{(1+\sin\theta\cos\phi)^2}{(1-\cos^2\phi\sin^2\theta)} \left\{ \sum_{j=1}^{N} A_j [\beta_{j+1} J_1(k\beta_{j+1}\sqrt{1-\cos^2\phi\sin^2\theta}) - \beta_j J_1(k\beta_j\sqrt{1-\cos^2\phi\sin^2\theta})] \right\}^2 . \tag{20}$$

From (1), the gain for the SPS spacetenna is

$$G(\theta,\phi) = \frac{4\pi K(\theta,\phi)}{P_T} \tag{21}$$

where P_T = input power.

The expression (20) for the radiation intensity is indeterminate for $\theta = \pi/2$, $\phi = 0$, which corresponds to the boresight direction. In this case it is not difficult to show the gain is

$$G(\pi/2,0) = \frac{2\pi^3}{\lambda^2 Z_o P_T} \left\{ \sum_{j=1}^{N} A_j \ (\beta_{j+1}^2 - \beta_j^2) \right\}^2 . \tag{22}$$

The actual SPS spacetenna is configured as discrete elements rather than a uniformly distributed amplitude. From (10) and (12), the pattern generated by the uniform distribution in β' gives $A_j J_0(k\rho'\sin\alpha)$ in each step. The residual between the uniform distribution and M discrete elements in the β'-direction is given by (Ma, 1974)

$$\text{Residual} = \left\{ \exp[iM(\tfrac{\pi}{2} - \beta') + (-1)^m \exp[-iM(\tfrac{\pi}{2} - \beta')] \right\} J_M(k\rho'\sin\alpha) + 2\cos(M\pi - 2M\beta') J_{2M}(k\rho'\sin\alpha) + \cdots . \tag{23}$$

It can be shown that, for large M, the error or residual in (23) is very small by using the asymptotic form for the Bessel functions in (23), and in the case of the SPS spacetenna, for $\alpha = \pi/2$, and a 500 meter dish radius with $\lambda = 0.12249$m, we find $J_M(Z) < 5 \times 10^{-3}$.

Table 4.1 gives the A_j and β_j currently being proposed for the SPS spacetenna (SPS System Definition Study, 1978).

The amplitudes in Table 4.1 were computed by multiplying the given power densities by Z_o (impedance of free-space). Substituting the A_j and β_j into (22) and performing the sum yielded a gain of 84.65 dB. If 3 dB is added to account for the fact that the actual SPS spacetenna radiates over one hemisphere and not a whole sphere, we obtain a final gain of 87.65 dB, in very close agreement with the gain of 87.46 dB given in the SPS System Definition Study (1978). In (22) we used a total input power of P_T = 6.85 GW.

Table 4.1 A_j and β_j for SPS spacetenna

j	A_j(volts/m)X 10^{-3}	β_j(m)
1	2.889	0
2	2.637	93.9
3	2.359	177.3
4	2.153	229.5
5	1.926	271.2
6	1.668	323.3
7	1.445	365.1
8	1.362	396.3
9	1.179	417.2
10	0.963	458.9
11	0	500.6

Figure 4.6 shows a plot of the SPS gain versus angle θ from boresight in the ϕ = 0 plane, for $89° \leq \phi \leq 95°$ with θ = 90° corresponding to boresight. Figure 4.7 shows more detail of the sidelobe structure for $93.440 \leq \theta \leq 93.640$, and Figure 4.8 shows the detail of the gain for $179 \leq \theta \leq 181$. Using program "Bigmain," NASA gives gains at θ = 0.080 of -57.3 dB, while the ITS program yields -57.4 dB. However, this is an estimate derived with ideal assumptions, and therefore may not be physically realizable. Today's experience with antennas would lead one to expect a gain at 90° from boresite around -10 dB.

Finally, concluding this section, we give two estimates of the attenuation and phase delay for moist and dry air (Liebe, 1977). At 2.45 GHz, at an altitude of 5 km and for 50% relative humidity, the attenuation is 0.003 dB/km and phase delay 8.68 radians/km, while for dry air the corresponding values are essentially zero.

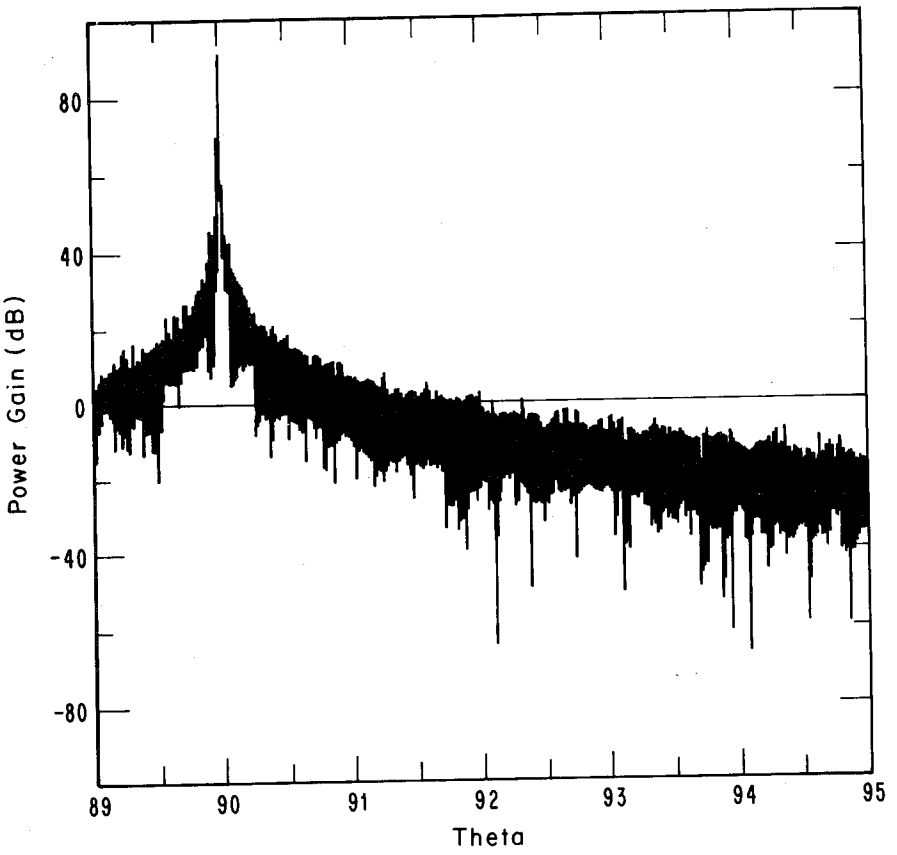

Figure 4.6. Gain versus angle from boresight. On-axis gain is about 87.65 dB.

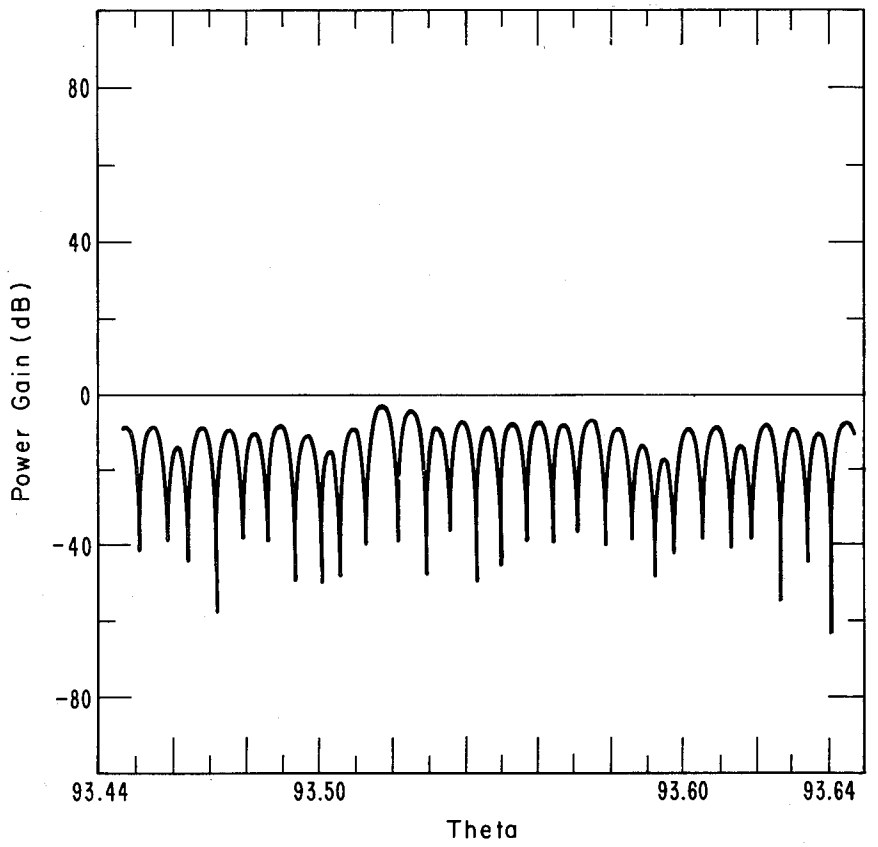

Figure 4.7. Gain versus angle from boresight showing sidelobe detail.

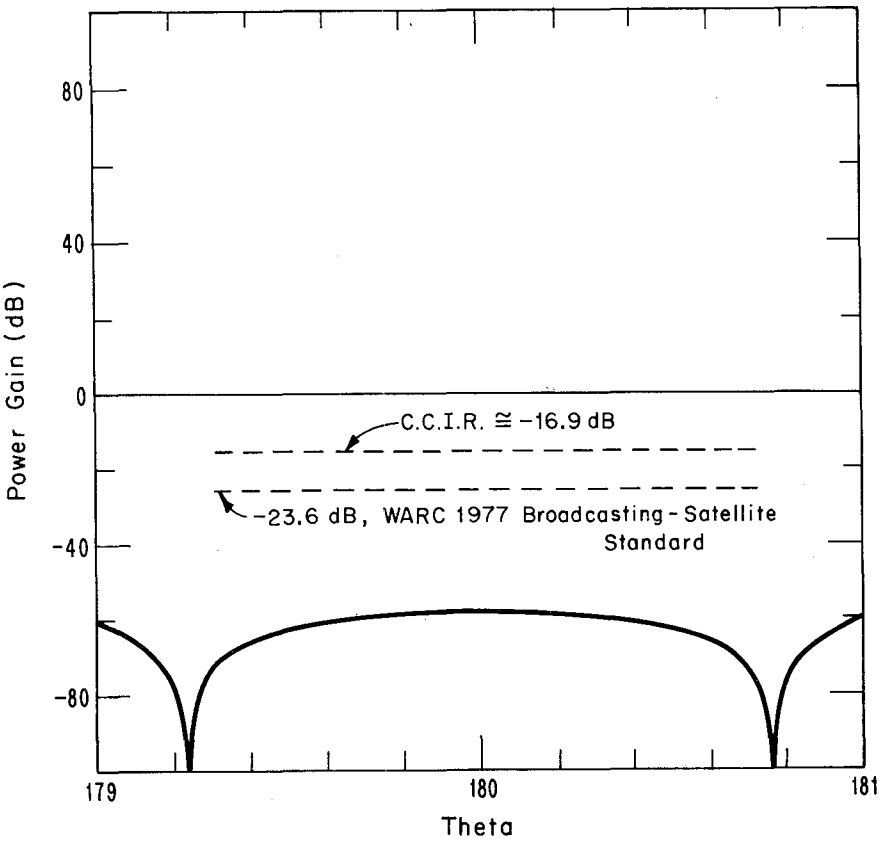

Figure 4.8. Gain versus theta for angles 90° from boresight.

5. PRELIMINARY ASSESSMENT

The initial hypothetical rectenna sites were identified by a previous study. Subsequent coordination with the NASA/MSFC Advanced Planning Office indicated an active study examining a hypothetical Mojave rectenna site. The initial EMC analysis exercise addressed this site so as to provide EM impact data to this site characteristic review and to contribute to the development of site selection criteria for NASA/DOE.

Figure 4.9 shows the Mojave site and the surrounding area that would be impacted by SPS emissions outside the rectenna enclosure. Figure 4.9 shows the fundamental main beam and sidelobe structure for the SPS using a 10 dB taper.

The rectenna site is shown with center at 35°8' North, 117°30' West. The rectenna covers an area roughly 150 km^2. The outer ellipse is roughly 78 km East-West by 100 km North-South and corresponds roughly to the scattered power density shown in Figure 4.10. Generally, in dealing with communications systems, field intensities measured at an antenna are given in microvolts per meter ($\mu V/m$). For high-power televisions or AM and FM broadcast stations, the field intensity beyond a mile, but within a few tens of miles, may be measured in millivolts per meter. Most likely for the average TV owner, the level of a field intensity measured at the home antenna would be in the microvolt per meter range. This will help to put the amount of energy beyond the rectenna site due to sidelobe structure in proper perspective.

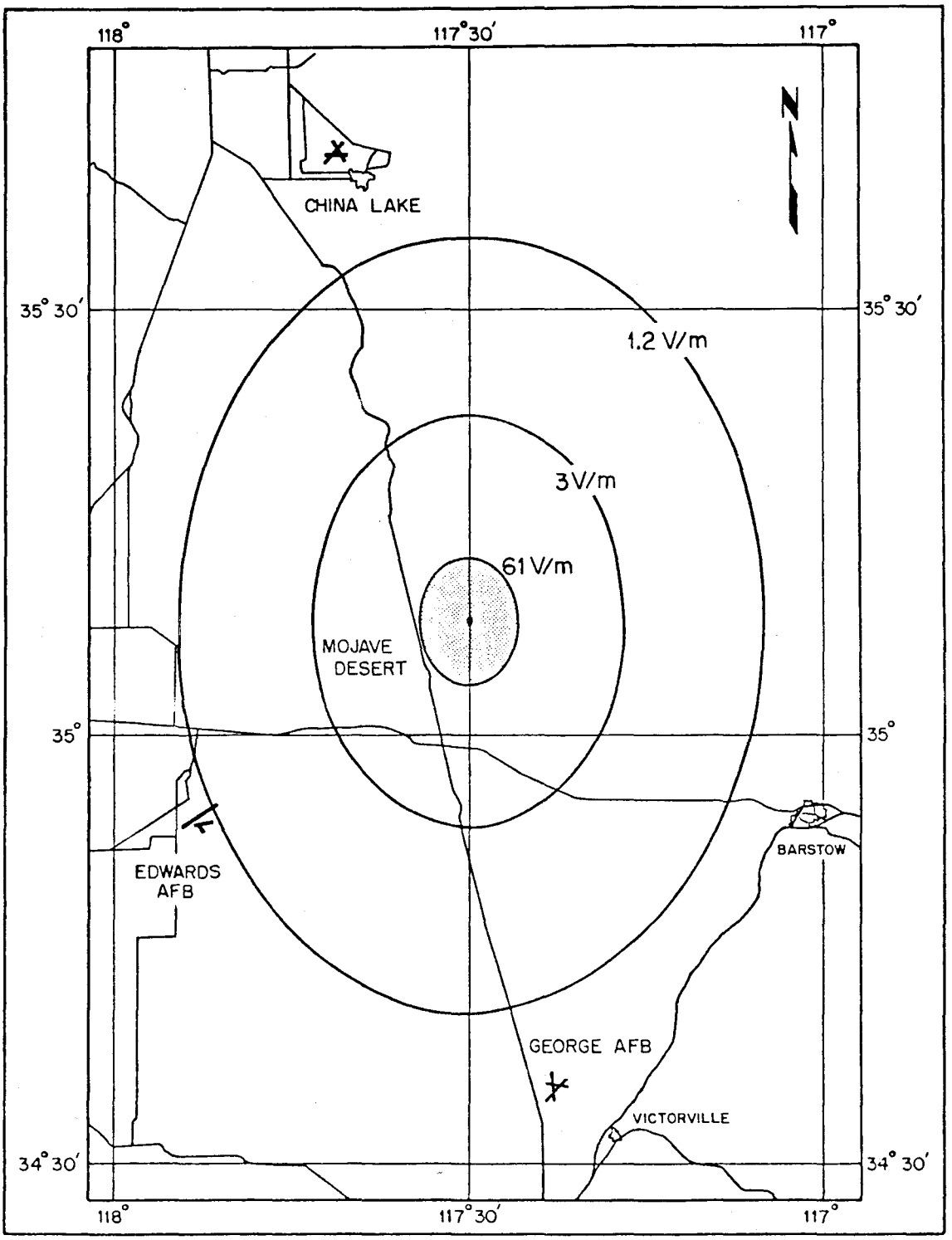

Figure 4.9. SPS microwave field intensities near the hypothetical Mojave rectenna site used for EMC analysis.

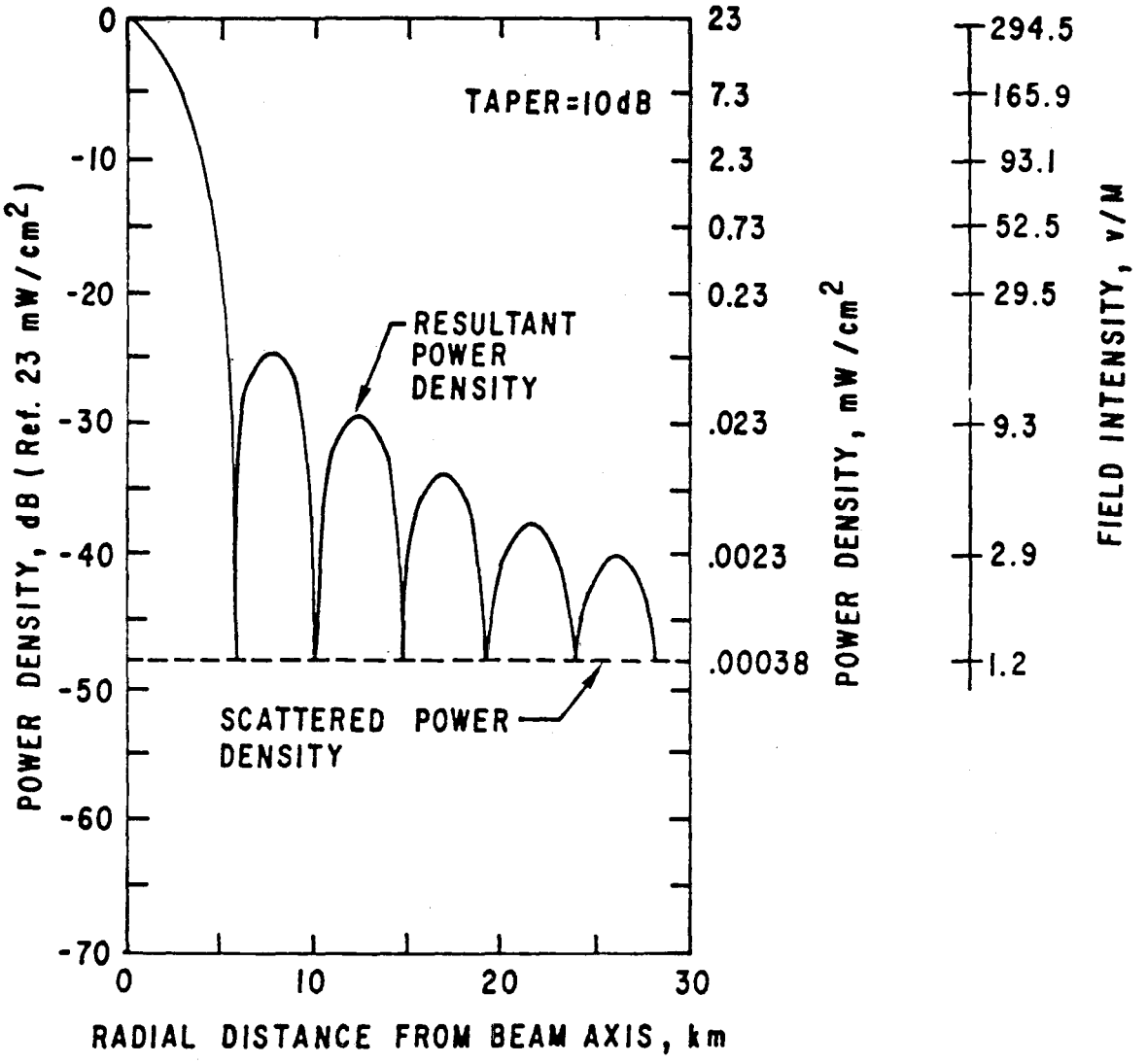

Figure 4.10. SPS microwave field strengths near rectenna sites.

Referring to Figure 4.10, the right-hand scale has two number values. One is power density in milliwatts per centimeter squared (mW/cm^2), and a corresponding scale is shown of field intensity in volts per meter (V/m) that an antenna might see. This represents a sizable input to communication systems operating within 100 km of the rectenna site. In addition to the EM field due to sidelobes present near a rectenna area is the power scattered from the main beam from media effects.

Analysis presented in this section is confined to the Mojave location insofar as received power calculations and tropospheric-caused interference are concerned. However, since the SPS concept presently envisions 60 SPS power-receiving rectenna configurations in the USA, other climates are being evaluated. The Mojave site represents one set of climatological conditions, there is no simple way to extrapolate the derived results to other, often more inclement, climates.

6. POWER LOSS AND BEAM REFRACTION AND SCATTER AT THE MOJAVE SITE

Part of the tasking involved with analysis of the Mojave site included estimating power losses from the main beam due to the atmosphere. This is in addition to estimating scattered energy from the main beam by atmospheric anomalies given in Sections 6.3, 6.4, and 6.5 which help characterize the EM energy surrounding the site for EMC analysis. The power loss analysis is given below rather than submitting it as a separate report.

Radio waves at a frequency of 2.45 GHz suffer little attenuation by the lower atmosphere of the earth. Gaseous absorption, due to both oxygen and water vapor absorption, will contribute no more than about 0.1 dB; rain absorption no more than another 2 dB. This total of 2.1 dB represents the worst case and, although small, gives a loss of 30% of the originally transmitted power. On the average, about 0.02 dB of attenuation is expected at a frequency of 2.45 GHz on a 30° elevation angle path to a satellite in a temperature climate characterized by a gaseous atmosphere with no rain. Even this, however, represents a 4.5% loss of power.

In the following subsections, the impact of the static atmosphere, rain, and sand or dust storms on the average received power from the SPS are analyzed for the Mojave site. It should be noted that this section and Section 6.3 are concerned only with atmospheric particulate effects. Effects of refractive index anomalies are discussed in Section 6.4 entitled "Power Scattered by Refractive Index Anomalies." At frequencies above 10 GHz, depolarization due to precipitation begins to be of some consequence, but generally not below 10 GHz. The critical frequency at which dust and sand depolarization is of any consequence is much higher than 10 GHz. Hence, depolarization effects are not considered herein.

The fluctuating component can be modeled as Gaussian if the fluctuations are small with respect to the mean, and many fluctuations are considered (Brooks and Carruthers, 1953). Given a mean and variance for each of the appropriate attenuation and phase delays, the computer random number generator, RANF, is utilized to prepare sample sets of gaussian-distributed fluctuations., These fluctuations are incorporated into a 10-minute sample rain or sand storm. The choice of a 10-minute sample is arbitrary, but a "complete" event has been incorporated into the interval; i.e., a rain storm begins and ends during the 10 minutes. Thus, the resultant average power loss during the event is hopefully a representative number. The model storm is sampled at a sufficiently large number of times, t, so that the average power results can be accurately represented and the average power loss obtained. These procedures are described in more detail in the following subsections.

6.1 Power Loss During a Desert Thunderstorm

A desert thunderstorm including rain effects only (i.e., ignoring the turbulence that is usually simultaneously generated) can be modeled from average annual distributions of rain rate by using existing ITS computer programs (Dutton, 1977; Janes et al., 1978). These programs were used to generate rain-rate distributions at 14 locations with rainfall patterns similar to the Mojave site and then obtain the corresponding distributions of attenuation, phase delay, and their variances on a satellite-earth path having an elevation angle $\theta_o = 49°$. These locations are: Phoenix, Tucson, Winslow, and Yuma, Arizona; Bakersfield, Bishop, and Sandberg Ranch, California; Silver City, Las Vegas, Elko, Ely, Reno, and Winnemucca, Nevada; and El Paso, Texas. The resultant distributions of the mean attenuation, $\bar{\tau}_g + \bar{\tau}_p$; rain attenuation standard deviation, σ_τ; mean phase delay, $\bar{\phi}_g + \bar{\phi}_p$; rain-caused phase delay standard deviation, σ_ϕ; and mean rainfall rate, R_o, were predicted for each of these locations. In the above, the subscripts g and p represent gaseous (clear air) results and precipitation (usually rain) results, respectively. The predicted results for all stations were then pooled, and values that are expected to be exceeded for the same percentage of a year, p, were grouped together. Then polynomial least-squares fits of the form (excluding fitting errors) were derived from the pooled data samples. (See the following equations.)

$$\bar{\tau}(P) = \bar{\tau}_y + \bar{\tau}_p(P) = \sum_{i=o}^{4} C_i [\bar{R}_D(P)]^i , \tag{24}$$

$$\sigma_\tau(P) = \sum_{i=o}^{4} C_{1+5} [\bar{R}_o(P)]^i \tag{25}$$

$$\bar{\Phi}(P) = \bar{\Phi}_g + \bar{\Phi}_p(P) = \sum_{i=o}^{4} C_{i+10}[\bar{R}_o(P)]^i \ , \tag{26}$$

and

$$\sigma_\tau(P) = \sum_{i-o}^{4} C_{i+15}\,[\bar{R}_o(P)]^i \tag{27}$$

were derived from the pooled data sample. In (24) through (27), C_0 through C_{19} are the coefficients of the fits. These fits were then used to obtain values for attenuation and phase delay for the distribution of mean rain rates, $\bar{R}_0(P)$, for the Mojave site. The $\bar{R}_0(P)$ values for the Mojave site were obtained by the interpolation techniques and USA-wide data base contained in FORTRAN program PREDIC (Dutton, 1977).

However, one question remains: what do annual distribution values have to do with a single, 10-minute thunderstorm event? By arbitrarily assuming that at certain times during a thunderstorm the rain-rate is in one-to-one correspondence with certain $\bar{R}_0(P)$ values, we can build a model thunderstorm. Specifically, if t is the time after the onset of a thunderstorm, we take several discrete values of $\bar{R}_0(P)$ for

$$0.01\% \leq P \leq 1\% \ , \tag{28}$$

and for these values set

$$\bar{R}_0(t = (1 \mp P)5\text{min}) = \bar{R}_0(P). \tag{29}$$

If we then fit a smooth curve* through the several values resulting from (29), we obtain the curve shown in Figure 6.1. This storm, as a result of incorporating low probability rain events (P = 0.01%), can be assumed to represent a severe storm at the Mojave rectenna site--close to a worst case situation.

Further in (31), if t = time after onset of a thunderstorm, we can now write, based on earlier assumptions:

$$\bar{\tau}_g + \tau_p(t) = \bar{\tau}_g + \bar{\tau}_p = Z(T)\sigma_\tau \ , \tag{30}$$

$$\bar{\phi}_g + \phi_p(t) = (\bar{\phi}_g + \phi_p) + Z(t)\sigma_\tau \ , \tag{31}$$

i.e., in terms of the parameters derived from $\bar{R}_0(t)$ of Figure 6.1 and (24) through (27) and a random standard normal deviate, Z(t), obtained (after appropriate uniform to Gaussian distribution transformation) from RANF**.

---

*Actually fit with a straight line for $P \geq 0.48$ and a fourth degree polynomial.

**Note that to use a normal distribution for $\tau_p(t)$ and $\phi_p(t)$, the condition $3\sigma_\tau \leq \bar{\tau}_p$ and $3\sigma_\phi < \bar{\phi}_p$, as discussed in Dutton (1977), should be met. This is because of the non-negative nature of $\tau_p(t)$ and $\phi_p(t)$.

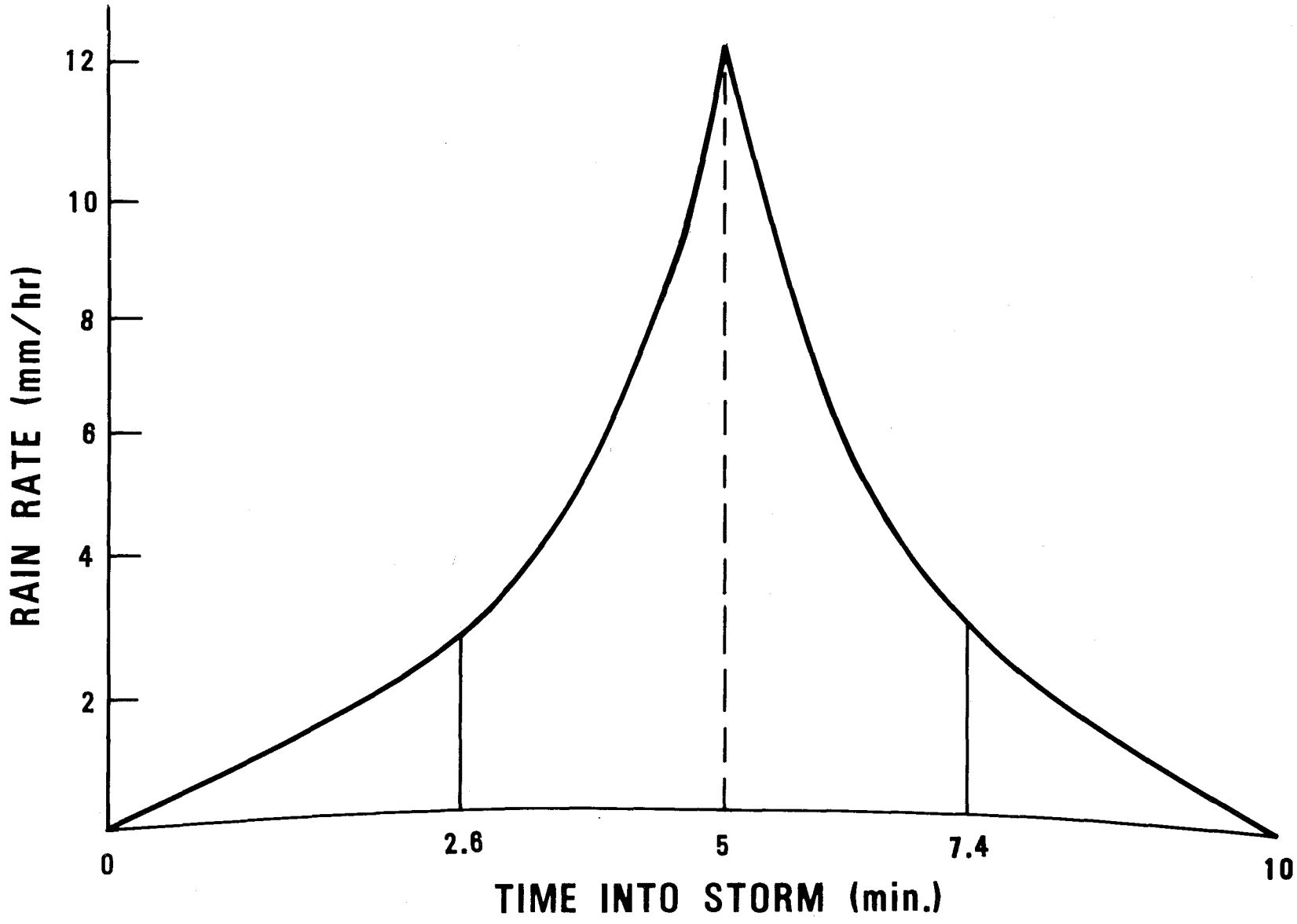

Figure 6.1. Rain rate in the model thunderstorm for the Mojave Desert rectenna site.

As mentioned earlier, if plane-wave reception can be assumed across the rectenna during a thunderstorm, the average power received from the SPS can be estimated by averaging over time (10 minutes), and the rain-caused phase delay will have no impact on this received power. However, the rectenna reception concept is not entirely conducive to this kind of assumption. It is currently proposed to acquire power through a series of dipole elements, 10 m x 25 m, mounted on ground screen panels. Each element may well contain 100 half-wave dipoles per m^2 over a ground screen. Through this array, power is converted to dc and bussed through power-summing apparatus for the entire rectenna. If we assume the total rectenna array is roughly 10 km x 10 km, this will mean that there are literally thousands of dipole receivers in each dimension. For our purposes, we shall assume that there are m dipoles in one dimension and n dipoles in the other dimension of the rectenna.

Now let us assume that the rain-rate produced by the thunderstorm has the "spherical cell" spatial distribution described in Dutton (1967) at any time, t, into the storm. This can be expressed as

$$\bar{R}(t,r) = \begin{cases} \bar{R}_o(t)\ [1 - \frac{r}{r_o}\ ]^{C_2} & r \leq r_o\ , \\ 0 & r > r_o\ . \end{cases} \tag{32}$$

In (32), r is the distance from the center of the storm to the $\bar{R}_o(t,r)$ isopleth; r is the radius of the total storm. Now let us assume that a 10-minute duration thunderstorm is centered directly over the rectenna, such as sketched in Figure 6.2, for the entire 10-minute interval. This hypothetical, static storm waxes and wanes while centered over the rectenna and, hence, represents a worst-case situation that is relatively easier to analyze than a storm with motion.

The total power, P_{fs}, received from a plane wave travelling through free space by the rectenna is

$$P_{fs} = \rho_{fs} A = nm\rho_{fs} A_b\ , \tag{33}$$

where

- A = total rectenna area (assumed rectangular) consisting of a matrix of n x m dipoles;
- A_b = effective boresight aperture area of a single dipole, with all A_b's assumed to be the same;
- ρ_{fs} = incident power density in free space.

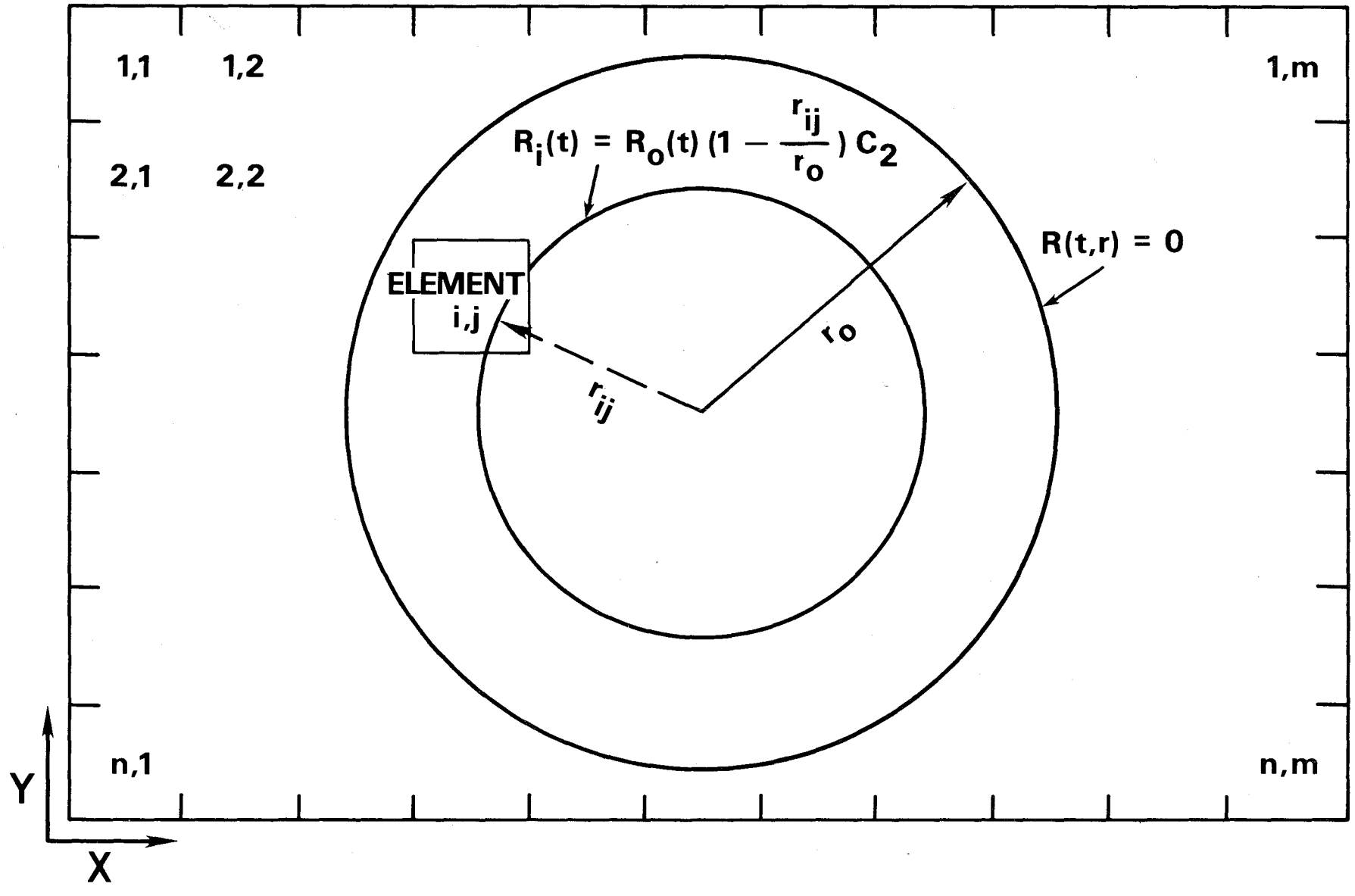

Figure 6.2. Sketch of the spherical cell model thunderstorm centered over the SPS receiving rectenna.

Referring now to Figure 6.3, we can see that, if the plane wave is now distorted by the atmospheric medium, the wave will be tilted by some angle θ_{ij} on the average over the antenna element (i,j) of length D in the dimension shown in Figure 6.3. If we let $\underline{E}_o$ be the received field, the power density ρ_{ij}, received by the (i,j) element is then

$$\rho_{ij} = \frac{|\underline{E}_o|^2}{\eta_o} \tag{34}$$

where η_o is the impedance of free space (essentially) and ρ_{ij} is the power density that would be received at (i,j) from a plane wave. Thus the received power, P'_{ij}, over the element (i,j) of an equivalent, untilted plane wave is

$$P'_{ij} = \rho_{ij} A_b \ , \tag{35}$$

and the actual received power, P_{ij}, is

$$P_{ij} = \rho_{ij} A'_b \ , \tag{36}$$

where A'_b is the actual antenna aperture for the tilted wave. For large distances, d, such as from the SPS to the rectenna, a spherical wave can be treated essentially as a plane wave, and we can use the transmission equation to write

$$P'_{ij} = \frac{P_t g_t}{4\pi d} \left(\frac{\lambda^2 g_r}{4\pi} \right) e^{-\tau(R_{ij})} \ . \tag{37}$$

In (37), P_t is the transmitted power, g_t is the main beam transmitting antenna gain, g_r is the boresight gain* ($\theta_{ij} = o$) of the element (i,j), λ is the operating wavelength (12.24 cm), and $\tau(R_{ij}) = \bar{\tau}_y + \bar{\tau}_y + \tau_p(t)$ is the atmospheric attenuation due to clear air and whatever rain rate, R_{ij}, as determined by (32), is present over the element (i,j). The average power, P_{ij}, received by the distorted wavefront over the element (i,j) can be written as

$$P_{ij} = \frac{P_t g_t}{4\pi d} \left[\frac{\lambda^2 g_r(\theta_{ij})}{4\pi} \right] e^{-\tau(R_{ij})} \ , \tag{38}$$

because, by noting Figure 6.3, it is clear that the element antenna is now receiving, on the average, at the angle θ_{ij}, instead of at boresight, so that g_r is replaced

*Assumed the same for all elements in the rectenna.

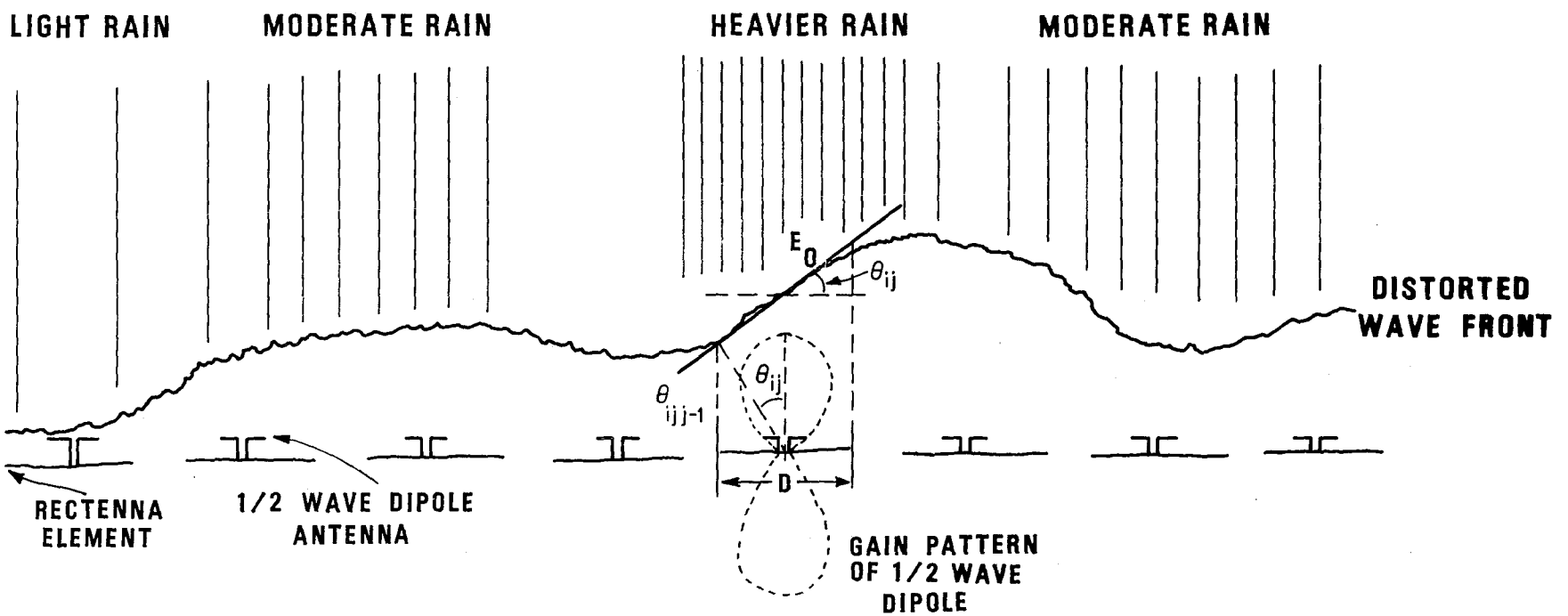

Figure 6.3. Cross section of the rectenna and a (originally) plane wave distorted by a rainstorm, sandstorm, or other atmospheric effects.

by $g_r(\theta_{ij})$. It can readily be shown that for a half-wave dipole (Blake, 1966, p. 174)

$$g_r(\theta_{ij}) = g_r \frac{\cos^2\left(\frac{\pi}{2}\sin\theta_{ij}\right)}{\cos^2\theta_{ij}} \tag{39}$$

where $g_r = 1.64$. We have not considered the effect of the ground screen, which, of course, will modify the result (39) some. This is because it turns out that θ_{ij} is so small as to yield essentially the same result regardless of pattern choice (see page 35). Substitution of (39) into (38) yields

$$P_{ij} = \frac{P_t g_t}{4\pi d^2}\left(\frac{\lambda^2 g_r}{4\pi}\right)\frac{\cos^2\left(\frac{\pi}{2}\sin\theta_{ij}\right)}{\cos^2\theta_{ij}}\, e^{-\tau(R_{ij})} . \tag{40}$$

The power received in free space, P_{ijfs}, over the antenna element (i,j) is the same as that over any other element, and can be obtained from the transmission equation as

$$P_{ijfs} = \rho_{fs} A_b = \frac{P_t g_t}{4\pi d^2}\left(\frac{\lambda^2 g_r}{4\pi}\right) . \tag{41}$$

Substituting this into (40) yields

$$P_{ij} = \rho_{fs} A_b \frac{\cos^2\left(\frac{\pi}{2}\sin\theta_{ij}\right)}{\cos^2\theta_{ij}}\, e^{-\tau(R_{ij})} . \tag{42}$$

The total received power, P, can then be expressed as

$$P = \rho_{fs} A_b \sum_{i=1}^{n}\sum_{j=1}^{m} \frac{\cos^2\left(\frac{\pi}{2}\sin\theta_{ij}\right)}{\cos^2\theta_{ij}}\, e^{-\tau(R_{ij})} \tag{43}$$

over the entire rectenna. The ratio, P/P_{fs} (the power at the rectenna actually received when passing through a stormy atmosphere to the total power that would be received in free space), can be compared to determine the fraction of power actually lost in the atmosphere. This ratio, using (33), is

$$\frac{P}{P_{fs}} = \frac{1}{mn}\sum_{i-1}^{n}\sum_{j=1}^{m} \frac{\cos^2\left(\frac{\pi}{2}\sin\theta_{ij}\right)}{\cos^2\theta_{ij}}\, e^{-\tau(R_{ij})} . \tag{44}$$

If we average (44) over the entire (10-minute) storm, sampling a total of H_p times during the storm, and we set

$$X_{kij} = \frac{\cos^2(\frac{\pi}{2} \sin \theta_{kij})}{\cos^2\theta_{ij}} \; e^{-\tau(R_{kij})} \quad , \tag{45}$$

then

$$\left(\frac{\overline{P}}{P_{fs}} \right) = \frac{1}{mnNp} \sum_{k=1}^{N_p} \sum_{i=1}^{n} \sum_{j=1}^{m} X_{kij} \; . \tag{46}$$

For all practical purposes, since θ_{kij} is minutely small over an area A_b, especially at 2.45 GHz,

$$X_{kij} \cong e^{-\tau(R_{kij})} \; ; \tag{47}$$

i.e., pure attenuation.

The problem with the solution (46) is its actual physical implementation into a computer software package when there are as many receiving elements (n and m both very large) as in the proposed Mojave rectenna configuration. An actual "DO loop" on the computer for very large n and m would be prohibitively expensive. However, it is possible to achieve representative results for (45) and the corresponding average received power through an inductive reasoning process based on computer results for small n and m. As n and m are slowly incremented from n = 1 and m = 1 for successive computer runs, it is observed that, by the time n = 11 and m = 11, the 10-minute average received power during a thunderstorm of fixed radius, r_o, shows virtually no change with increases in n and m. Whether or not this implies that the average received power is approaching an asymptote near the n=m=11 value is not at all certain from the above reasoning. However, in what follows, an argument that the actual average received power value can be closely approximated for relatively small m and n for the largest model thunderstorm (r_o = 5 km) will be presented.

As stated previously, the rectenna array is assumed to be roughly 10 km by 10 km in horizontal dimensions on the earth's surface, and that n and m are both odd integers. Then the storm will be centered over the rectenna as in Figure 6.2. If in Figure 6.2 we label the "row" (or horizontal) dimension x and the "column" (or vertical) dimension y, then the horizontal component $\Delta_j x$ from the "center" element to the element (i,j) is (for equal-sized elements)

$$\Delta_j x = \left(\frac{m+1}{2} \right) - j \left| \frac{10}{m} \right. . \tag{48}$$

Similarly, for the vertical component $\Delta_i y$ from the center element,

$$\Delta_i y = \left| \left(\frac{n+1}{2} \right) - i \right| \frac{10}{n} \quad . \tag{49}$$

Note these results are in kilometers, since the "10" in (48) and (49) represents the 10 km rectenna dimension. Whence we can define a discrete set of r's in (32), r_{ij}, such that

$$r_{ij}^2 = (\Delta_j x)^2 + (\Delta_i y)^2 \quad . \tag{50}$$

From (32), the heaviest rain rate falls at the center element ($r_{ij} = 0$), and from Figure 10 it is plain to see that the greatest change in rain rate is between the center element and an adjacent element. There will be a spacing Δr between elements in the rectenna at which the rain-rate differential, ΔR, is sufficiently small that no appreciable phase difference contribution will accrue, and, thus, there will essentially be, for computation purposes, no need to reduce element spacing further, since all the significant phase differences due to rain will have been taken into account. If this phase differential is inconsequential between the center element and an adjacent element, it should be inconsequential between any other pair of adjacent elements. We are concerned with adjacent elements because we are interested in investigating the spacing at which adjacent elements in (46) are still distinguishable. Further, this will aid in determining the maximum number of elements needed in the rectenna power analysis since, from (48) and (49), the smallest spacing, $\Delta r.$, between adjacent elements is

$$\Delta r = \frac{10}{n} \left(\text{or } \frac{10}{m} \right). \tag{51}$$

The largest rain-rate difference, ΔR, between the center element and an adjacent element is, from (32),

$$\Delta R = \overline{R}_o(t = 5 \text{ min})\left[1 - \left(1 - \frac{\Delta r}{r_o}\right)\right] \quad . \tag{52}$$

We have chosen $\Delta R = 1$ mm/hr as the rain-rate difference below which the difference between adjacent elements in (46) is inconsequential. From differentiation of (26), we find that the largest $\Delta\phi$ resulting from a $\Delta R = 1$ mm/hr for Mojave conditions is

$$\Delta\phi \tilde{=} 1.35^\circ \quad . \tag{53}$$

An analysis of (45) using (53) shows that phase differences contributing to the tilt angle θ_{ij} in (45) caused by a $\Delta R = 1$ mm/hr amount to only about one part in 10^4, which implies that phase differences for $\Delta R = 1$ mm/hr do not affect (46) unless more than 4 decimal place accuracy is required. Hence the approximation (47) results.

The following analysis is in terms of the effective minimum number of elements, m and n, needed to analyze results in (46) to within the above stated accuracy for ΔR = 1 mm/hr. However, the accuracies mentioned above also show that the following analysis is probably not needed so far as the Mojave site is concerned, and that, for all practical purposes, phase change considerations could be ignored altogether --a conclusion borne out by the results in Table 6.1.

Table 6.1

Predicted Normalized Total Power Received at the Mojave Rectenna Over a Ten-Minute Interval for Various Storm Sizes

Storm radius, r_o(km)	Normalized Received Power $\overline{(P/P_{fs})}$	Standard Deviation of Normalized Received Power, S_p
1.0	0.9728_1	6.20×10^{-5}
2.5	0.9728_0	7.93×10^{-5}
5.0	0.9727_2	1.76×10^{-2}

The following analysis is presented because in heavier rainfall regimes (not the Mojave site) it may have application.

For ΔR = 1 mm/hr accuracy, we set (52) to

$$\overline{R}_o\ (5)[1-\ (1-\frac{r}{r_o})^{1.56}]\quad 1\ \text{mm/hr.}, \tag{54}$$

Since, at the Mojave site, $\overline{R}_o(5)$ = 8.05 mm/hr c_2 = 1.5626, substituting these values in (54), we arrive at the inequality

$$\Delta r \leq 0.0814\ r_o\ . \tag{55}$$

In other words, 0.0814 r_o is the largest distance over which computations have accuracy to rain-rate differences of 1 mm/hr.

The effective number of "elements," m' and n' in width and length, respectively, can be defined as the number of 1 mm/hr increments along any given dimension of the rectenna. Let us now assume (as is current planning) that the rectenna is more circular in appearance, with diameter D = 10 km. Since, for an assumed r_o = 5 km storm, the number of 1 mm/hr increments, I, along the diameter is

$$I = \frac{D}{\Delta r}\ , \tag{56}$$

we obtain

$$I(\text{-m' or n'}) = \frac{2r_o}{\Delta r}\ . \tag{57}$$

Using (55), then, we obtain

$$m' \text{ or } n' \geq \frac{2}{0.0814} = 25; \tag{58}$$

i.e., a minimum of 25 elements should provide accuracy to 1 mm/hr (4 decimal places) in a computation of (46). Smaller storm sizes or larger rain-rate increments will reduce this minimum number probably to the value n'=m'=11 that was most cost-effective in calculating (46) on the computer. As a check on using the m'=n'=11 number for an m and n in (46), one value of m'=n'=25 was run and found to be essentially unchanged from the m'=n'=11 value to 3 signicant figures.

Table 6.1 shows the results of average received power computations for the model thunderstorm in thunderstorm cells of various radii, r_o, at 2.45 GHz for the Mojave rectenna site. Note that each 0.01 of normalized power loss translates into 60 megawatts of power loss, assuming a free space received power of 6 gigawatts over the entire rectenna.

6.2 Power Loss in Desert Sand and Duststorms

Again we shall model a desert sandstorm on the basis that suspended sand and dust particles only affect the SPS beam, and that turbulence, which is often generated simultaneously, will be ignored. Also, we shall again treat a "worst case" model sandstorm configuration. Based on the work of Idso et al.,(1972), we shall now assume that a severe (worst case) sandstorm is 2.5 km in height and is about 15 km in diameter. These storms tend to have an inverted dish shape, but we shall assume a perfectly cylindrical storm. As a consequence, the model sandstorm is of a homogeneous character when assumed centered over the rectenna and, thus, does not present the element-to-element variability problem discussed in the last section for thunderstorms. More attention would have been given to the inhomogeneity case if the impact of the model sandstorm had been the same order of magnitude as that of the thunderstorm. However, the sandstorm impact is much less.

Dust and sand particulate matter diameters, D, even in storms where the diameters average > 100μ, are still less than 0.05 cm. Since at 2.45 GHz the wavelength, λ, is 12.24 cm, it is clear that Rayleigh region formulas ($\pi D/\Lambda << 1$) are applicable when calculating the bulk complex refractive index of the dusty medium (assuming spherical particles). Hence, for the case of mean specific attenuation (attenuation per unit length), $\bar{\alpha}_d$, due to atmospheric dust is

$$\bar{\alpha}_d(\text{dB/km}) = 0.51919 \frac{\varepsilon_2}{(\varepsilon_1 + 2)^2 + \varepsilon_2^2} \frac{\overline{M}}{\rho} f_{\text{GHz}} \quad , \tag{59}$$

where f_{GHz} = frequency in gigahertz, $\bar{M}$ is the mean dust particle concentration in grams per cubic meter (g/m^3), ρ = density of particle in g/m^3, and ε_1 and ε_2 are the real and imaginary parts of the complex dielectric constant of dust at f_{GHz}. If we now follow CCIR Document 5/209-E, dated 31 May 1977, we obtain the results shown in Table 6.2.

Table 6.2

Dielectric Constants and Densities of Duststorm Particles

	ε_1	ε_2	ρ_3 g/cm
sand	3.8	0.038	2.63
clay	5.1	0.24	2.32

If we assume that the mean sandstorm consists of a particle 1/2 clay and 1/2 sand, we now have $\varepsilon_1 = 4.45$, $\varepsilon_2 = 0.139$, and $\rho = 2.425\ g/cm^3$. In the same CCIR document we find the relationship

$$M(g/m)^3 = 1660 \times 10^{-6} (\bar{V}_{ft})^{-1.43} \quad , \tag{60}$$

where $\bar{V}_{ft}$ is the mean visibility in feet through the sandstorm. Substituting this expression into (59), we obtain

$$\bar{\alpha}_d(dB/km) = \frac{1.35986 \times 10^{-3}}{\rho} \frac{\varepsilon_2 \bar{V}_{ft}^{-1.43}}{(\varepsilon_1 + 2)^2 + \varepsilon_2^2} f_{GHz} \ . \tag{61}$$

If we assume that (61) applies to all α_d's and V's (not just their mean values), then

$$\sigma_{x_d} \simeq \left[\frac{1.9446 \times 10^{-3}}{\rho} \frac{\varepsilon_2 \bar{V}_{ft}^{-2.43}}{(\varepsilon_1 + 2)^2 + \varepsilon_2^2} \right]^2 \sigma_v \ f_{GHz} \ , \tag{62}$$

where σ_v^2 is the variance of V in ft^2 and $\sigma_{\alpha_d}^2$ is the variance of α_d in $(dB/km)^2$.

Sandstorms are arbitrarily defined as occurring for meteorological measurement purposes when the visibility, V, is reduced to 1000 m or less. Thus, we shall arbitrarily define these percent times, P, during a sandstorm:

$$P(V<1000m) = 99.99\% \ , \tag{63}$$

$$P(V< 0.5m) = 0.01\% \ . \tag{64}$$

The percentage in (64) is based on the results given in El-Fandy (1953). For a normally distributed set of visibilities, then,

$$\bar{V} + 3.179\,\sigma_v = 1000\ \text{m}, \tag{65}$$

$$\bar{V} - 3.719\,\sigma_v = 0.5\ \text{m}, \tag{66}$$

$$\bar{V} = 500.25\text{m}, \tag{67}$$

$$\sigma_v = 134.38\text{m}. \tag{68}$$

The expression for the received signal, $S_d(t_o + t)$, during the model sandstorm can be written analogously to (46) where all symbols are as defined earlier, except t, time, is now referenced to the onset of a 10-minute duration sandstorm rather than a thunderstorm. Because the sandstorm is assumed homogeneous, and plane-wave reception is assumed, Φ_g and $\Phi_d(t)$ do not play a role in the analysis of the power loss at the rectenna due to the model sandstorm. However, discussion of them is included herein for completeness. Analogous to (30) and (31), we can write:

$$\bar{\tau}_g + \tau_d(t) = (\bar{\tau}_g + \bar{\tau}_d) + z(t)\sigma_{\tau_d}\ , \tag{69}$$

$$\bar{\Phi}_g + \Phi_d(t) = (\bar{\Phi}_g + \bar{\Phi}_d) + z(t)\sigma_{\Phi_d}\ , \tag{70}$$

where $\bar{\tau}_d$ and $\bar{\Phi}_d$ are the mean values of attenuation; $\tau_d(t)$ and $\Phi_d(t)$ are the attenuation and phase delay due to dust or sand particles, respectively; and σ_{τ_d} and σ_{Φ_d} are the standard deviations of $\tau_d(t)$ and $\Phi_d(t)$, respectively. These means and standard deviations can be obtained in terms of the means and standard deviations of the specific attenuation, $\alpha_d(t)$, and specific phase delay, $\phi_d(t)$, from

$$\begin{vmatrix} \bar{\tau}_d \\ \sigma_{\tau_d} \\ \\ \bar{\Phi}_d \\ \sigma_n \end{vmatrix} = \ell \begin{vmatrix} \bar{\alpha}_d \\ \sigma_{x_d} \\ \\ \Phi_d \\ \sigma_n \end{vmatrix}\ , \tag{71}$$

where ℓ, the path length through the sandstorm from the Mojave rectenna to the SPS, is given by

$$\ell = 2.5\ \text{CSC}\ 49^\circ = 3.3\ \text{km}. \tag{72}$$

Also in (71), the values of $\bar{\Phi}_d$ and σ_{Φ_d} can be obtained from the same Rayleigh region assumptions used to obtain (26) and (62). This results in

$$\bar{\phi}_d(\text{rad/km}) = \frac{5.21864\text{x}10^{-5}}{\rho} \frac{(\varepsilon_1-1)(\varepsilon_1+2)+\varepsilon_2^2}{(\varepsilon_1+2)^2+\varepsilon_2^2} f_{GHz} V^{-1.43} \qquad (73)$$

and

$$\sigma_{\phi_d} = \left[- \frac{7.46266\text{x}10^{-5}}{\rho} \frac{(\varepsilon_1-1)(\varepsilon_1+2)^2+\varepsilon_2^2}{(\varepsilon_1+2)^2+\varepsilon_2^2} f_{GHz} V^{-2.43} \right]^2 \sigma_v , \qquad (74)$$

using previously defined symbols.

Calculations indicate that the model sandstorm contributes very little to either attenuation or phase delay at 2.45 GHz; the average received normalized power in (46) is essentially that in the static, clear air atmosphere; viz,

$$\left(\frac{\bar{P}}{P_{fs}} \right) \cong e^{-\bar{\tau}_g} = 0.9728. \qquad (75)$$

Expression (75) certainly implies that the preceding sandstorm analysis was largely unnecessary--had this been known a priori.

6.3 Power Scattered by Sandstorms and Duststorms

We shall assume that the average reflectivity (Bean et al., 1970) of a volume of discrete atmosphere scatterers, $\bar{\eta}(\lambda)$ in km^{-1} ,

$$\bar{\eta}(\lambda) = \frac{\pi^5}{4} |K|^2 Z \times 10^{-7} \; (\eta^-(\lambda) \text{ in } km^{-1} , \qquad (76)$$

is isotopic, λ cm, Rayleigh, and equal to the backscatter value. The value

$|K|^2 = \left| \frac{\varepsilon(\lambda) - 1}{\varepsilon(\lambda) + 2} \right|^2$ where $\varepsilon(\lambda)$ is the complex index of refraction at wavelength λ (frequency f) and Z is the so-called "radar reflectivity factor." We can obtain $\varepsilon(\lambda)$ from CCIR Doc 5/209-E, May 31, 1977, which gives the dielectric constant $\varepsilon_s(\lambda)$ of sand, density 2.63 g/cm^3, as

$$\varepsilon_s(\lambda) = \varepsilon_{s1} = i\varepsilon_{s2} = 3.8 - i(3.8 \times 10^{-2}) \qquad (77)$$

and the dielectric constant $\varepsilon_c(\lambda)$ of clay, density 2.32 g/cm^3, as

$$\varepsilon_c(\lambda) = \varepsilon_{c1} - i\varepsilon_{c2} = 5.1 - i(2.4 \times 10^{-1}) . \qquad (78)$$

These results apply to 10 GHz, but following Harvey (1963), we shall assume the results are constant and valid from 0.4 to 10 GHz, since they correspond roughly to his results for that range. Now,

$$|K|^2 = \left[\frac{(\varepsilon_1 - 1)(\varepsilon_1 + 2) = \varepsilon_2^2}{(\varepsilon_1 + 2)^2 + \varepsilon_2^2)}\right]^2 + \left[\frac{3\varepsilon_2}{(\varepsilon_1 + 2)^2 + \varepsilon_2^2}\right]^2$$

$$\simeq \left(\frac{\varepsilon_1 - 1}{\varepsilon_1 + 2}\right)^2 \quad \text{for } \varepsilon_2 << \varepsilon_1. \tag{79}$$

Table 6.3 will indicate the rather extreme sandstorm conditions we intend to use to illustrate the scattering of unwanted power from the SPS at the California desert site. As before, we shall assume that each dust particle in a storm is an even mixture of sand and clay, and assume that, therefore, sand and clay each contributes one-half the extreme distribution density (equivalent to liquid water content) M given by Ahmed and Auchterlonie (1976). It is possible (but not at all certain) that the mean between sand and duststorms represents the average storm of the windblown soil type.

Table 6.3

Representative Sandstorm Conditions

Value	Source	Sand	Clay
$\bar{D}$	CCIR DOC 5/209-E, May 1977	0.015 cm	0.008 cm.
M_{max}	CCIR DOC 5/209-E, May 1977	$1.12 \times 10^{-2} g/cm^3$	$1.82 \times 10^{-3} g/cm^3$

Furthermore,

$$Z = \sum_{t_i} D_i^6 \text{ per } m^3 = N\bar{D}^6 \tag{80}$$

where N = number of particles per m^3 and $\bar{D}$ is some average diameter of a (spherical) dust particle. Whence* $N_s = 2.41 \times 10^9\ m^{-3}$, and $N_c = 2.93 \times 10^9\ m^{-3}$ using Tables 6.1 and 6.2, so that (80) yields $Z_s = 2.75 \times 10^4\ mm^6/m^3$, and $Z_c = 7.68 \times 10^2\ mm^6/m^3$. Again s subscripts are for sand and c subscripts are for clay. The power density, $\bar{p}_r$, scattered by a sandstorm from the SPS main beam can be written as:

$$\bar{p}_r = p_i \left[\frac{\sigma(\lambda)}{4\pi L_r^2}\right] \quad \text{(no attenuation assumed)}, \tag{81}$$

*$M = 4/3\pi\ \rho\ (\bar{D}/2)\ N$, whence

$N = 6/M\pi\bar{D}^3\rho$ ρ = Particle Density .

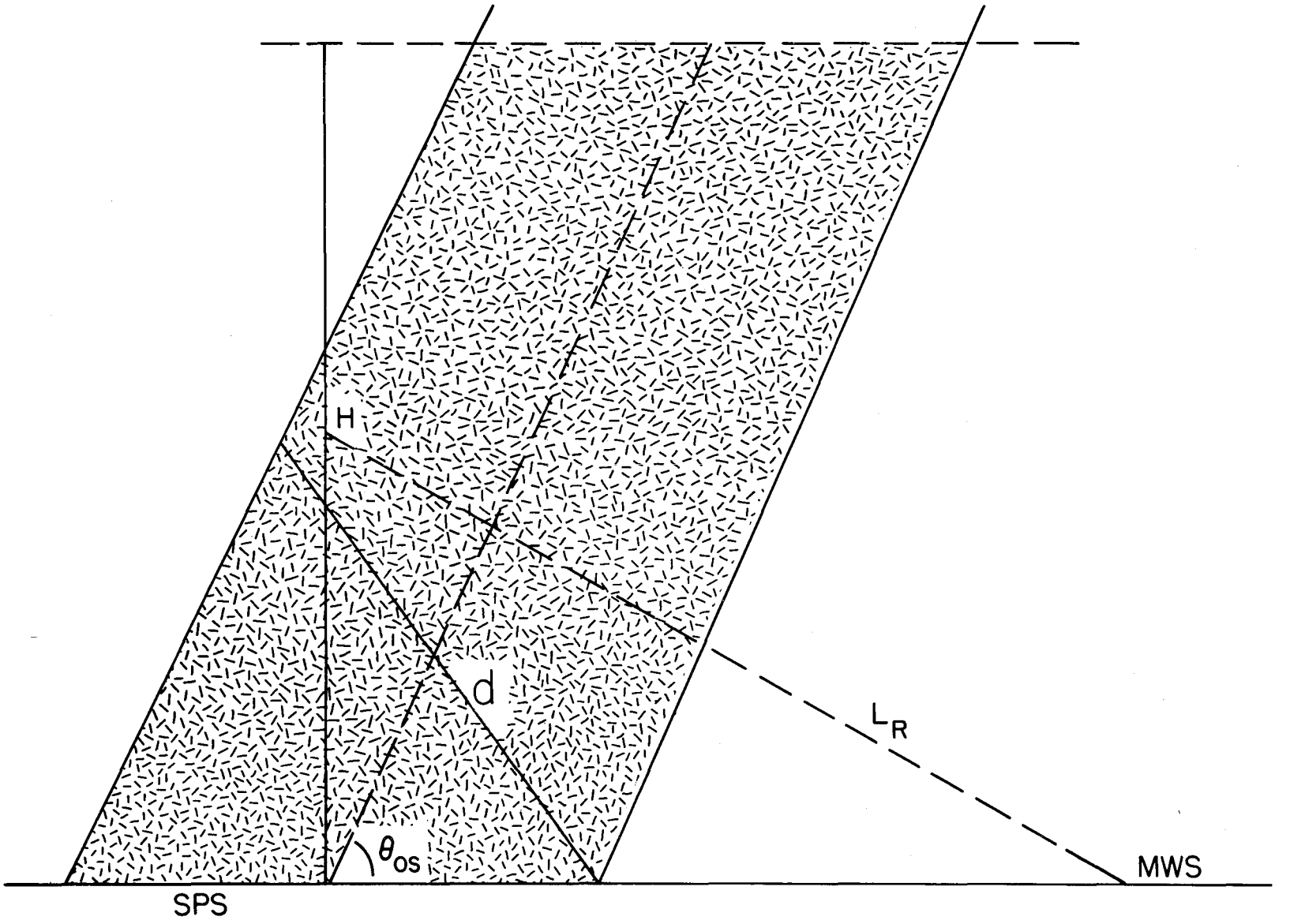

Figure 6.4. Scatter geometry over a plane earth.

where p_i is the incident SPS power density, 16 mw/cm^2 or 16 x 10^7 w/km^2,

$$\sigma(\lambda) \cong \bar{\eta}\ (\lambda)\ V \quad , \tag{82}$$

$$V \cong \pi 4(\delta_r L_r)^2\ d\ \csc\ \theta \quad . \tag{83}$$

In (81), (82), and (83), as depicted in Figure 6.4, V is the common volume intersection of the SPS main beam and the main beam of a co-channel microwave system (MWS) receiver on the earth's surface--assumed a complete intersection of the two beams and completely filled by particles, d is the diameter of the SPS main beam at V, assumed $\cong$ 5.6 km at the 3 dB points, $\lambda \cong$ 12.24 cm (2.45 GHz), δ_r is the beamwidth of the MWS main beam, L_r is the distance from the MWS to V, and θ is the scattering angle.

Referring to Figure 6.5, if θ_{os} is the elevation angle of the rectenna, θ_{or} the elevation angle of the MWS, and x is the distance between the SPS and MWS, then clearly,

$$\theta = \theta_{os} + \theta_{or} \tag{84}$$

and

$$L_r = x \sin \theta_{os} \csc \theta \quad . \tag{85}$$

Substituting into (81) yields

$$\bar{p}_r \cong \frac{p_i\ \eta^{2(\lambda)}}{16}\ \delta_r^3 d\ \csc\ (\theta_{os} + \theta_{or}) \ . \tag{86}$$

So that clearly as θ_{or} decreases, csc $(\theta_{os} + \theta_{or})$ increases, and so does $\bar{p}_r$ for any given set of the other parameters of ( ) fixed. Thus, low altitude sandstorms (and they are usually not over 1 km in height) might pose a more serious problem for systems viewing at low θ_{or}. If a system, such as isotropic system, has no δ_r^2 , the scattering volume is simply the volume of the duststorm in the SPS main beam, and if H is the height of the storm, then

$$V = \frac{\pi}{4}\ (d\ \csc\ \theta_{os})^2\ \ H. \tag{87}$$

The average distance to V is then

$$L_r \cong \begin{cases} \sqrt{(H/2)^2 + x^2} & \text{(88a)} \\ x = \text{for } x \gg H \quad . & \text{(88b)} \end{cases}$$

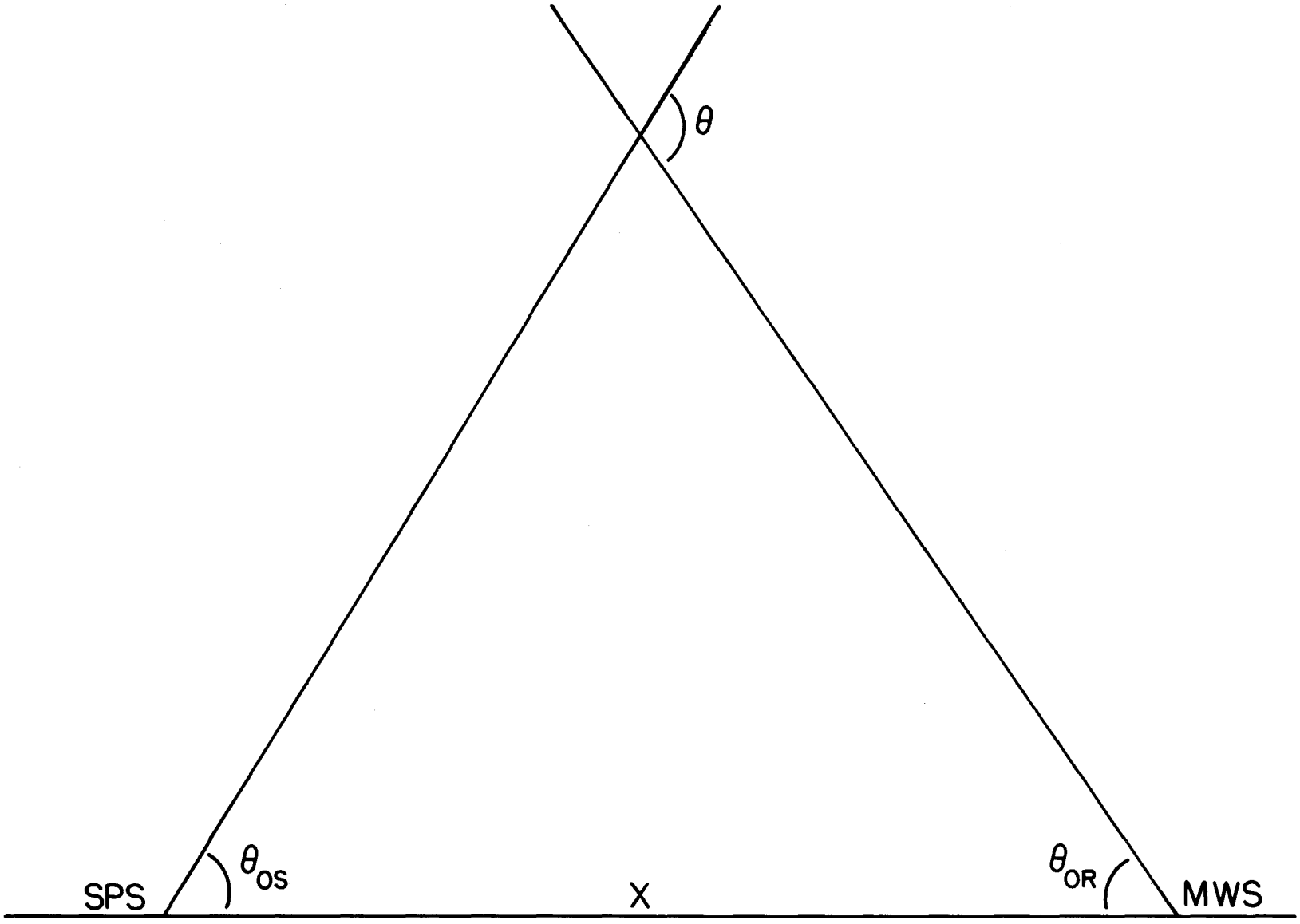

Figure 6.5. Scatter geometry over a plane earth.

If x is 20 km, then, since H is usually 1 km, we will assume (88b) holds. Also, for the Mojave rectenna site, $\theta_{os} = 49.2°$. Then (81) becomes

$$\bar{P}_r \cong \begin{cases} \dfrac{P_i\, \eta(\lambda)\, d^2 H}{16\, [(H/2)^2 + x^2\,]}\, \csc^2 \theta_{os} & (89a) \\ \dfrac{P_i\, \eta(\lambda)\, d^2 H}{16x^2}\, \csc^2 \theta_{os}\,, \quad x \gg H\,. & (89b) \end{cases}$$

For the initial consideration of the Mojave rectenna site, representative distances, x, are given in Table 6.4.

Table 6.4

Distances to Various Sites from the Mojave Rectenna Site

Location	x
SPS - China Lake Airstrip	64 km
SPS - Downtown Barstow	51 km
SPS - Edwards AFB Airstrip	43 km
SPS - Restricted Area R 2524	53 km
SPS - George AFB Airstrip	61 km

The distances in Table 6.4 imply the use of (89b).

Let us now evaluate a severe sandstorm. Let us assume that the reflectivity, $\eta(\lambda)$, of the common volume, V, is the sum of $\eta_s(\lambda)$ and $\eta_c(\lambda)$, the sand and clay reflectivities of per volume particle content assumed earlier*. Hence,

$$\eta(\lambda) = \eta_s(\lambda) + \eta_c(\lambda) = \frac{\pi^5}{\lambda^4 cm} \times 10^{-7}\, (|K_s|^2\, Z_s + |K_c|^2\, Z_c)\ \mathrm{km}^{-1}. \qquad (90)$$

We shall now compute the power density scattered by a volume of windblown sand to a isotropic antenna via (89b), which should represent close to a worst case for those potential MWS sites listed above. These values are shown in Table 6.5. Values used for the various parameters are those discussed previously.

*Note that this assumption is generally not the same as assuming a dust particle composed of 1/2 sand and 1/2 clay.

Table 6.5

Power Scattered by Sandstorms at the Mojave Rectenna Site

MSW Site	$\|K_s\|^2$	$\|K_c\|^2$	$\eta(\lambda)(km^{-1})$	$\bar{p}_r(w/km^2)$	$\bar{p}_r(mw/cm^2)$
China Lake Airstrip	0.233089	0.334226	9.09×10^{-6}	1.21	1.21×10^{-7}
Downtown Barstow				1.91	1.91×10^{-7}
Edwards AFB Airstrip				2.69	2.69×10^{-7}
Restricted Area R2524				1.77	1.77×10^{-7}
George AFB Airstrip				1.34	1.34×10^{-7}

Again, note that these results are for scattering by the largest possible common volume--that formed by the sandstorm and the SPS main beam. Turning our attention now to duststorms, El-Fandy (1953) assessed the mean diameter, $\overline{D}$, of dust particles in these storms and found it to be considerably smaller than the values for sand of CCIR Document 5/209-E, dated May 31, 1977, used earlier. El-Fandy (1953) also reports the value of N. For the duststorms observed, these values are

$$\overline{D} = 2.0\mu = 20. \times 10^{-13} \text{ mm} \tag{91}$$

$$N = 550 \text{ cm}^{-3} = 5.5 \times 10^{8} \text{ m}^{-3} . \tag{92}$$

From (80), we obtain

$$Z = 3.52 \times 10^{-8} . \tag{93}$$

If all other values are kept the same* as they were to achieve Table 6.4, then we obtain the results shown in Table 6.6.

These values certainly appear less formidable than those of Table 6.5. The reason for the vast difference in $\bar{p}_r$ in the two tables is basically the difference in size of the dust particles as opposed to the size of sand and clay particles. In the International Classification of Dusty Atmospheres (El-Fandy, 1953), the diameter of duststorm particles must be ≤ 10 , and the diameter of sandstorm particles must be > 100 .

---

*Except $|K|^2$ will be assumed $\dfrac{|K_s|^2 + |K_c|^2}{2} = 0.283658$

Table 6.6

Power Scattered by Duststorms at the Mojave Rectenna Site

MWS Site	$\eta(\lambda)(km^{-1})$	$\bar{p}_r(w/km^2)$	$\bar{p}_r(mw/cm^2)$
China Lake Airstrip	1.36×10^{-17}	1.82×10^{-12}	1.82×10^{-19}
Downtown Barstow		2.86×10^{-12}	2.86×10^{-19}
Edwards AFB Airstrip		4.03×10^{-12}	4.03×10^{-19}
Restricted Area R2524		2.65×10^{-12}	2.65×10^{-19}
George AFG Airstrip		2.00×10^{-12}	2.00×10^{-19}

Clearly, however, the kind of storm likely to occur at the SPS sites will depend on the kind of soil found in the area and the size of the soil particles. There is a monumental lack of information on which kind of storm--duststorm or sandstorm--tends to prevail in an area. Distinction between the two is based on such parameters as particle size or visibility, neither of which is a wholly satisfactory indicator. Unfortunately, as we have seen, the distinction is important to EM scattering at microwave frequencies. The need for a great deal more work in this area is clearly implied, and a great deal more information and data needs to be accumulated. Section 6.6, however, discusses the frequency with which wind occurs near the Mojave site, and these results should be strongly correlated with the occurrence of sand and duststorms over a year's time--although not in one-to-one correspondence.

6.4 Power Scattered by Refractive Index Anomalies

Scattering by refractive index fluctuations, termed "angel echoes," is likely to be the most prevalent scatter effect at arid area rectenna sites, particularly during the summer. This effect is likely to be aggravated by the heating of the rectenna, causing thermal instabilities in a cone of atmosphere directly over it.

A common appearance of these refractive-index-caused angel echoes is as a band or layer on a radar scope. A frequently used expression for the reflectivity of these layers [actual expression is polarization dependent](Crane, 1970) is

$$\eta(\lambda) \cong 0.39^{*}\, C_n^2\, \lambda^{-1/3} \,. \tag{94}$$

*Values may vary from about .33 to .39.

The results in Table 6.6 can be interpreted as "per kilometer of height" power density scattered, since they were computed for a 1 km high duststorm, and (89b) is proportional to H. Angel-echo reflection can extend for several kilometers, but an exact upper limit is not known.

However, if we compute angel-echo power density scattered per kilometer of height by (89b), we can compare the effective scattering of angel echo turbulence with that of duststorms. This will compare two major atmospheric scattering effects that are likely to affect the Mojave desert site.

In addition, we shall compute angel-echo turbulence scatter for a layer 3 km thick extending from the surface, as an estimate of extreme conditions. Further, we shall take a large value of $C_n^2 = 10^{-11}$ $cm^{-2/3}$ [which is very unlikely to extend the full 3 km (Battan, 1973)] to compute both the per kilometer and the 3-km scattered power densities. Isotropic scatter is again assumed. These results are given in Table 6.7.

Table 6.7

Power Scattered by Angel Echoes at the Mojave Rectenna Site

MWS Site	$\eta(\lambda)$ (km^{-1})	$\bar{p}_r$ per km ($w/km^2/km$)	$\bar{p}_r$ for 3 km layer (w/km^2)	$\bar{p}_r$ for 3 km layer (mw/cm^2)
China Lake Airstrip	1.69×10^{-7}	2.26×10^{-2}	6.78×10^{-2}	6.78×10^{-9}
Downtown Barstow		3.56×10^{-2}	1.07×10^{-1}	1.07×10^{-8}
Edwards AFB Airstrip		5.00×10^{-2}	1.50×10^{-1}	1.50×10^{-8}
Restricted Area R2524		3.92×10^{-2}	9.87×10^{-2}	9.87×10^{-9}
George AFB Airstrip		2.49×10^{-2}	7.47×10^{-2}	7.47×10^{-9}

Angel echoes caused by thermal instability are usually strongest in the late afternoon, and virtually nonexistent in the pre-dawn. Naturally, they are more prevalent in the summer than in other seasons of the year.

6.5 Scattering by Other Mechanisms

Other atmospheric scattering and multipath mechanisms include:

1) rain,
2) melting hail,
3) atmospheric layers (multipath),
4) atmospheric aerosols.

In addition, energy will be scattered by the terrain and by the rectenna itself. The latter two, however, will only be diffuse multipath, with little specular component at the sizable angle of arrival (θ_{os} = 49.2°) of the SPS energy. Even this diffuse component could cause trouble, however, and it remains to be evaluated. It has not been done here, since it is a rather complicated calculation procedure. Rain (Item 1 above) and hail (Item 2 above) would be serious problems if the rectenna were located some place other than the California desert. Even here there may be occasional serious degradation at nearby MWS sites when rain does occur, because desert rains do tend to be "gullywashers."

Suppose we take Bakersfield, CA, as representative of rainfall to be found in the Mojave SPS receiving site vicinity (although it is still a considerable distance away and somewhat lower in elevation)*. Bakersfield receives a rain rate of about 9.1 mm/hr on the average of about 1 hour per year, and at the extreme (1 year out of 200) it receives 17.3 mm/hr for 1 hour during a year. For about 5 minutes of an average year, Bakersfield incurs 19.3 mm/hr of rain rate, and incurs 47.2 mm/hr at the 1 out of 200 year extreme for 5 minutes of that year. Based on the work of Dutton (1977), we can predict, roughly, the height, HTOP, of a storm that will produce the aforementioned rain rates at the earth's surface. Since rain scatter is approximately isotropic (latest CCIR thinking), we can use the relationship

$$Z = 200R^{1.6} \quad , \tag{95}$$

where R is the rain rate at mid-storm [for use in (37a) and (38b) only], HTOP/2. Then (95) can be used in (76) to estimate rain storm reflectivity, from whence $\bar{p}_r$ in (38b) can be obtained. This results in Table 6.8, based on Bakersfield data, for average conditions, and in Table 6.9 for extreme, 99.5% confidence (1 year out of 200) conditions.

Results in both Tables 6.8 and 6.9 are based on the commonly used (i.e., Battan, 1973) value of

$$|K|^2 \cong 0.93. \tag{96}$$

It can be seen from the various tables for the few minutes per year that the rain rates are expected--if the Bakersfield results are truly representative--that rain scatter is then far the most potent scattering mechanism. This could have an impact on systems with high reliability requirements. Then, however, such systems could be expected to be highly directive, whence equation (86) would have to be used in lieu

*Note that this rainfall representation is <u>not</u> the same as the model thunderstorm used in Section 2.1.

Table 6.8

Power Scattered by Average Rainstorms at the Mojave Rectenna Site

MWS Site	Z (mm^6/m^2)		$\eta(\lambda)$ (km^{-1})		$\bar{p}_r$ (w/km^2)		$\bar{p}_r$ (mw/cm^2)	
	1 hr/yr	5 min/yr	1 hr/yr	5 min/yr	1 hr/yr	5 min/yr	1 hr/yr	5 min/yr
China Lake Airstrip	6.84×10^3	2.28×10^4	8.67×10^{-6}	2.89×10^{-5}	5.27	20.7	5.27×10^{-7}	2.07×10^{-6}
Downtown Barstow					8.30	32.5	8.30×10^{-7}	3.25×10^{-6}
Edwards AFB Airstrip					11.70	45.8	1.17×10^{-7}	4.58×10^{-6}
Restricted Area R2524					7.69	30.1	7.69×10^{-7}	3.01×10^{-6}
George AFB Airstrip					5.80	22.7	5.80×10^{-7}	2.27×10^{-6}

Table 6.9

Power Scattered by Extreme Rainstorms at the Mojave Rectenna Site

MWS Site	Z (mm^6/m^2)		$\eta(\lambda)$ (km^{-1})		$\bar{p}_r$ (w/km^2)		$\bar{p}_r$ (mw/cm^2)	
	1 hr/yr	5 min/yr	1 hr/yr	5 min/yr	1 hr/yr	5 min/yr	1 hr/yr	5 min/yr
China Lake Airstrip	1.91×10^4	9.54×10^4	2.42×10^{-5}	1.21×10^{-4}	17.0	105.1	1.70×10^{-6}	1.05×10^{-5}
Downtown Barstow					26.7	165.5	2.67×10^{-6}	1.66×10^{-5}
Edwards AFB Airstrip					37.6	232.8	3.76×10^{-6}	2.33×10^{-5}
Restricted Area R2524					24.8	153.2	2.48×10^{-6}	1.53×10^{-5}
George AFB Airstrip					18.7	115.7	1.87×10^{-6}	1.15×10^{-5}

of (89b). Hence, the true seriousness of rain scatter is clearly also a problem in need of much greater and more detailed investigation.

Melting hail is usually present in every thunderstorm--convective type situation--to which the Bakersfield numbers used in Tables 6.8 and 6.9 pertain. Melting hail, however, because of the sparsity of the number of particles vis-a-vis rain in a given volume of atmosphere, is expected to give results 2 or 3 orders of magnitude lower than the results of Tables 6.8 and 6.9.

The efforts of trapping and multipathing by atmospheric layers should be inconsequential, because the angle of arrival of the energy, $\theta_{os} = 49.2°$, is much larger than the critical angle for layer trapping.

Atmospheric aerosols consist of diminutive particles roughly 0.1μ in diameter (Fraser, 1959). At that size, the scattering impact is even less than that for the duststorm scattering shown in Table 6.6.

This analysis shows the significance of scattered energy from the power beam to the surrounding areas of the rectenna site does not add significantly to that energy present due to sidelobe structure. In the analysis given here, the scattered energy ranges from 10^{-19} mw/cm^2 for duststorms to 10^{-5} mw/cm^2 for extreme rainstorms. The peak sidelobe energy at the given areas of Table 6.4 ranges from 10^{-4} mw/cm^2 which is the dominant microwave energy component for EMC considerations.

6.6 The Significance of Wind

For many clear air (and perhaps even some precipitation) scattering effects, the presence or the lack of wind is often a good indication of which kind(s) of effects are present. It should be noted that <u>some effects</u>, such as turbulence and a duststorm, <u>can easily exist simultaneously</u>. Other indicators, such as visibility, are also good indicators, but wind is probably the most frequently tabulated by meteorological services--although not always in the same way.

The most useful tabulation is wind velocity, because from that one can get some idea of the critical velocity (El-Fandy, 1953) at which duststorms and/or sandstorms can initiate. For instance, Oliver (1945) found that the mean critical velocity could be as low as 16 mph.

There are recordings (USNWS, 1969) of the mean number of days per year the surface wind is >15 mph (17 kts) at three of the sites of interest in the California desert--and they are all substantial. Table 6.10 indicates these results.

Table 6.10

Mean Days/Year Winds >15 mph Recorded

Location	Time of Day (LST) 0400	1000	1600	2200	Windiest Month
China Lake Airstrip	23.4	29.7	87.9	46.7	March
Edwards AFB Airstrip	14.6	36.2	114.6	22.9	May
George AFB Airstrip	8.4	29.5	81.0	12.6	April

From Table 6.10, it appears that spring is the windy season, and late afternoon is the windiest time of day--neither observation being particularly surprising. If data on temperature can be combined with the wind data, some indication of the formation of angel-echo scatterers may be possible. Hot, windy days would seem the most conducive to angel formation.

Lack of wind can be a useful indicator in that it may imply the presence of a stable, stratified atmosphere. This knowledge could help appraise the ducting and atmospheric multipathing tendencies of the atmosphere, although we have not concerned ourselves with these problems herein for reasons stated earlier.

7. SYSTEM PERFORMANCE EVALUATION

This section presents a summary of the potential effects of SPS illumination on the types of EM and electronic systems operated within 150 km of the proposed Mojave rectenna site. Identification of EM systems was accomplished primarily through a retrieval from the NTIA Spectrum Allocation and Assignment files and data from FCC commercial license records. Other electronic systems (sensors, computers) were identified through contact with transportation, utility, and pipeline organizations and operators in the California Mojave area, southwestern Nevada, northwestern Arizona, the California Communications Department, and the City and County of Los Angeles Telecommunications Agency.

Retrieval from the federal files included systems within a 145 km x 145 km boundary around the Mojave rectenna site, and operating frequencies between 15 MHz and 5 GHz. A total of 813 government systems and 685 civilian authorizations were identified within these boundaries.

For purposes of this environmental assessment, the equipment/system categories identified in the file retrieval are as listed:

1. Military Development and Operational Test and Evaluation.
    a. Instrumentation radars - conical scan and monopulse modes.
    b. Traffic monitor/control radars.
    c. Radar transponders.
    d. Radar signal and functional replicators.
    e. Wideband monitor receivers with recognition/decision software scan and instantaneous frequency modes.
    f. Television cameras for target position track.
    g. EM system operational monitors - multiple wideband receivers with processing software.
    h. Range command/control communications nets.
    i. Range telemetry communications networks.
2. Industrial Communications.
    a. Utility network command/control and telemetry.
    b. Pipeline network command/control and telemetry.
    c. Water resource telemetry.
    d. Multiplexed carrier networks - two major service systems.
3. Transportation Support Systems.
    a. Railroad mobile equipments - yards and enroute complex.
    b. Air traffic control network.
    c. Emergency services - mobile, base station, and relay equipments - medical and general emergency applications.
    d. Railroad "car condition" monitors.
4. Public Service Communications.
    a. State of California backbone network (law enforcement, resource management, emergency communications).
    b. Law enforcement systems - state, county, city - mobile, relay, and base station equipments.
    c. Forest service units.
    d. Fire and government emergency systems - county and city operations.
    e. Common carrier networks - telephone, data, television services - remote area voice links.
5. Specialized Services.
    a. Space tracking and monitoring facilities (Goldstone area).
    b. Railroad hump radars.

The China Lake and Edwards AFB test ranges include various radar, command/control and telemetry, and optical tracker/ scanner systems. For specific applications, infrared (IR) trackers may be employed for moving surface vehicles and airborne vehicles having low radar cross section and not accommodating a transponder.

A major expansion is distributed minicomputer and microprocessor application for instrumentation and event command functional control, and various data verification and formatting and network control requirements. Remote computer control capabilities will be required for complex interactive system operations (e.g.,

multispectral recognitions and assessment, computer managed mission profiles), as well as more effective data processing and range instrumentation facility utilization. Data security improvements in the control and data networks will also be served through the distributed processors.

The instrumentation and communications equipment types deployed at the military test ranges are listed.

1. Radars -

   FPS-16
   FPS-105
   TPQ-39
   M-33
   MSG-3A
   MPS-19
   NIKE AJAX
   NIKE HERCULES.

2. Television Cameras -

   Plumbicon units mounted on radar antennas for tracking aid, and mounted on high terrain pedestals for multiple camera target tracking.

3. Command/control and Telemetry -

   UHF FM multiplexed analog, L and S band FM multiplexed. All receivers use monopole low gain antennas.

Enhanced radar capabilities anticipated within a 5 to 10 year period include on-axis track modes (including digital prediction filter for range gate and pedestal angle control), phased array units for simultaneous multiple target track and integrated event control and telemetry, and simultaneous multiple frequency track modes to minimize multipath errors. For tests involving complex electronic warfare (EW) scenarios, an increased use of time and event sequenced multiple frequency modes will be required to assure instrumentation compatibility with equipment and procedures being evaluated. Compatibility and short-period accuracy considerations will increase SHF applications.

Communications evolution is expected to include increased microwave operations because of data channel requirements expansion. With the use of distributed processors for instrumentation control, preliminary data processing and formatting will be accomplished at remote modes before transmission to a central facility. Ultimately, frequency division multiplex (FDM) will be replaced by time-division multiple-access (TDMA) modes to accommodate high data rates and maximize spectrum utilization efficiency. When operating communication systems in high interference environments with severe accuracy and data rate requirements, atmospheric and fiber optical links will be utilized.

Scanning or staring optical sensors are expected to be increasingly used for spatial tracking in high-accuracy requirements, particularly in complex EM environments. The probable communications application was cited previously. Passive tracking (skin or exhaust plumes) with modulated sources will use scanning (vidicon, orthicon, plumbicon) and staring sensor modes (cooled semiconductor, charge coupled devices) for visual spectra or IR band detection.

Distributed processors at minicomputer and microprocessor levels will involve communications and sensor control (data acquisition, verficiation, formatting, network control, sensor orientation and lock cycling, hand-over management) and various levels of data processing. Modular elements will be interconnected by dedicated cables or through the microwave channels.

7.1 Receiver Evaluation

Range safety and mission operating area uncertainties (aircraft flight paths, missile trajectories, etc.) require that instrumentation radar and communication receivers operate without restriction covering any direction over the upper hemisphere. A tracking antenna could therefore have the main beam or principal side lobes pointed at the SPS source. Considering the Mojave site location and the China Lake and Edwards AFB distances and intervening terrain, the SPS interference is principally from the direct fundamental illumination. The direct second harmonic is reduced $\sim$ 70 to 80 dB. The fundamental power density contours around the rectenna site are plotted in Figure 4.9. These are based on only the spacetenna pattern, not including any scatter or refractive distortion of the power beam.

The radar and communications receiver performance scoring process is diagrammed in Figures 7.1 and 7.2, indicating the desired and interference signal inputs and functional measurement points. Receiver effects because of the SPS interferer include channel noise and intermodulation products at the higher SPS amplitudes into the input amplifier and/or first mixer. Specific performance scoring criteria for radar and communications receivers are listed below. Communications criteria are identified for analog and digital modes.

RADAR

a. Target detection range: skin and cooperative target modes.
b. Radar lock delay.
c. Target track error.
d. Loss of track probability.

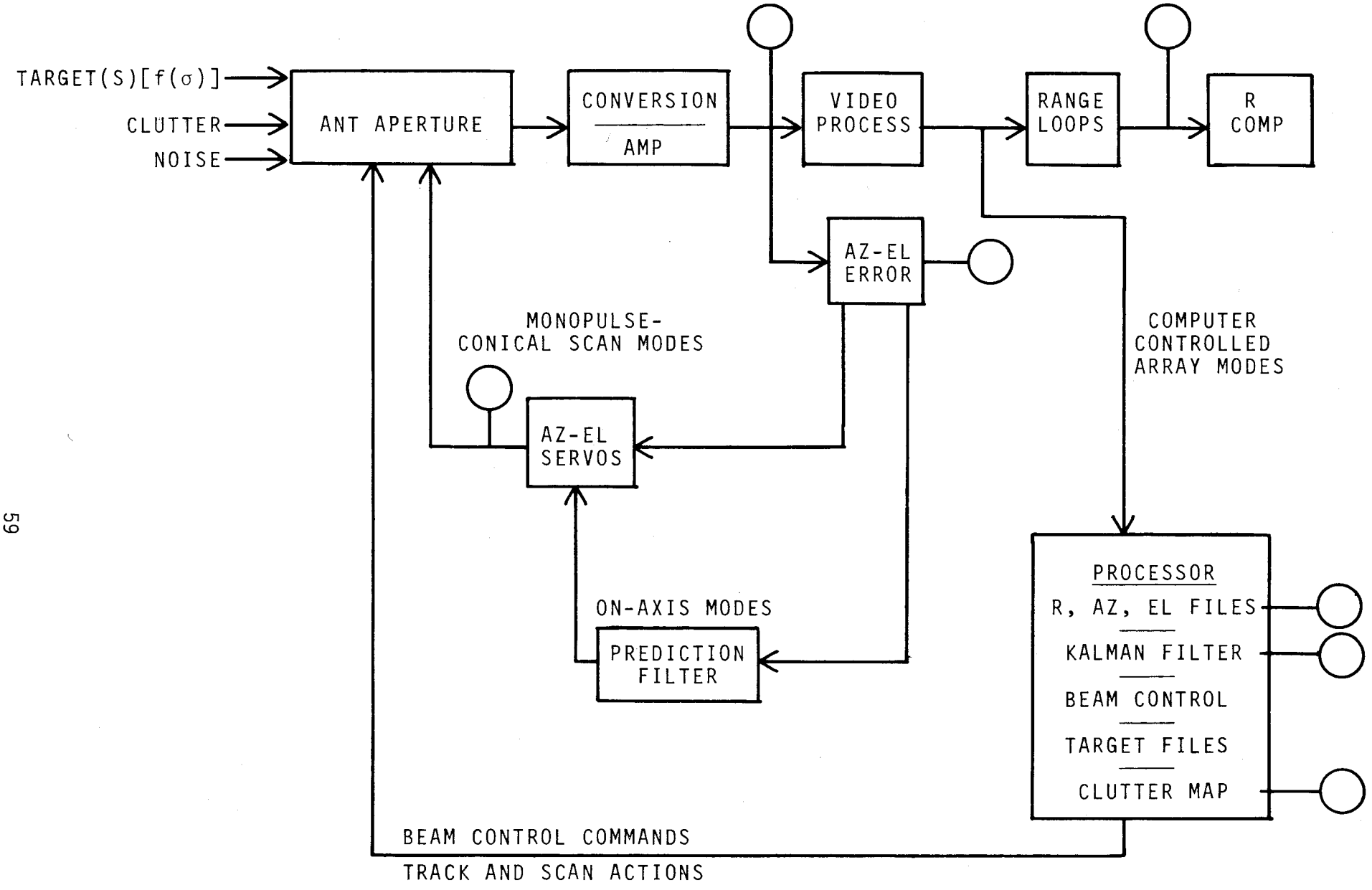

Figure 7.1. General radar functional diagram -
Mechanical antenna and computer controlled array modes.

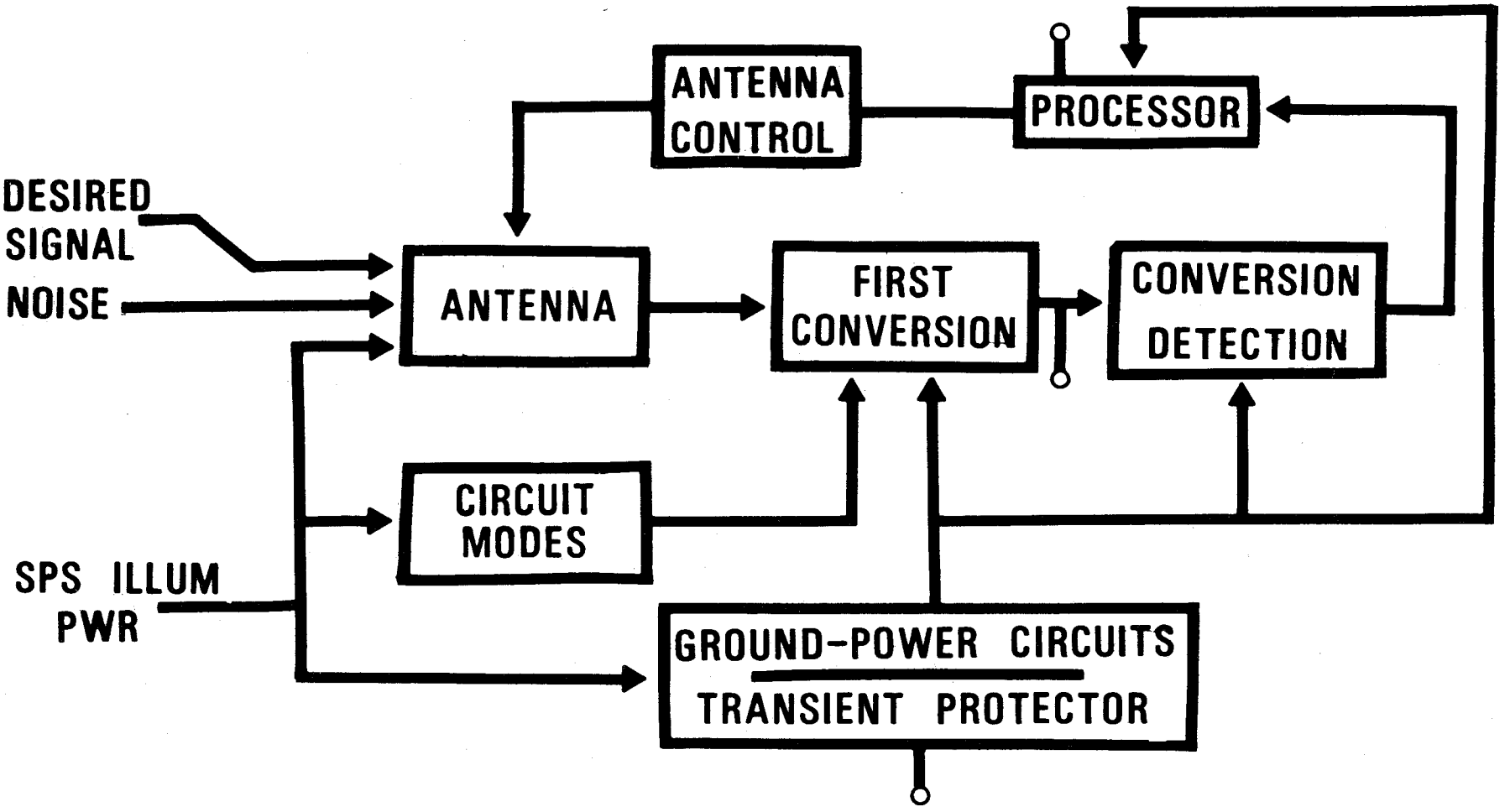

Figure 7.2. General EM receiver-signal and energy coupling.

COMMUNICATIONS

a. Signal acquisition delays.
b. Signal errors - Analog mode
  DMUX cross coupling
  data errors
- Digital mode
  BER sync noise and loss
  address error
  data error

When testing radar systems, the signal-to-noise ratio measured at the radar signal detector inputs was varied from a level corresponding to minimum detectable radar cross section (smallest target that can be detected when skin tracking) or corresponding to transponder power from lowest detectable signal to mid-range amplitudes when tracking a target with an active on-board tracking source. Noise and intermodulation spectral densities were tabulated for various signal-to-SPS interference combinations.

A representative operational event diagram for a test range radar is presented in Figure 7.3. This diagram indicates target detection, control data, and safety alarm data requirements. The performance criteria relates to the characteristics included in Section 7.5.

A typical operations diagram for a test range command/control relationship to hand over between training sensors (radar, TV camera or IR scanner) is indicated in Figure 7.4. Similar command/control relationships are identifiable with vehicle guidance data, target destruct actions, or chase aircraft control.

When testing communication systems, the desired signal was varied from minimum viable signal at the receiver to average link signal amplitudes. An interfering signal in the 2.45 GHz frequency range was introduced to the systems under test. Noise and intermodulation spectral densities were measured and tabulated for various S/I combinations.

Commercial and industrial communications receivers indicate nearly identical responses for S/I ratios in the 10 to 20 dB range. The principal predetection response involved induced noise with an amplitude in the range of 0 to 3 dB higher than comparable military FDM equipment. This difference is attributed to shielding and electrical grounding design because of the more stringent requirements of military specified equipment. At lower S/I ratios (1 to 6 dB), the level at which intermodulation products were first detectable was about 2 dB earlier with commercial equipment.

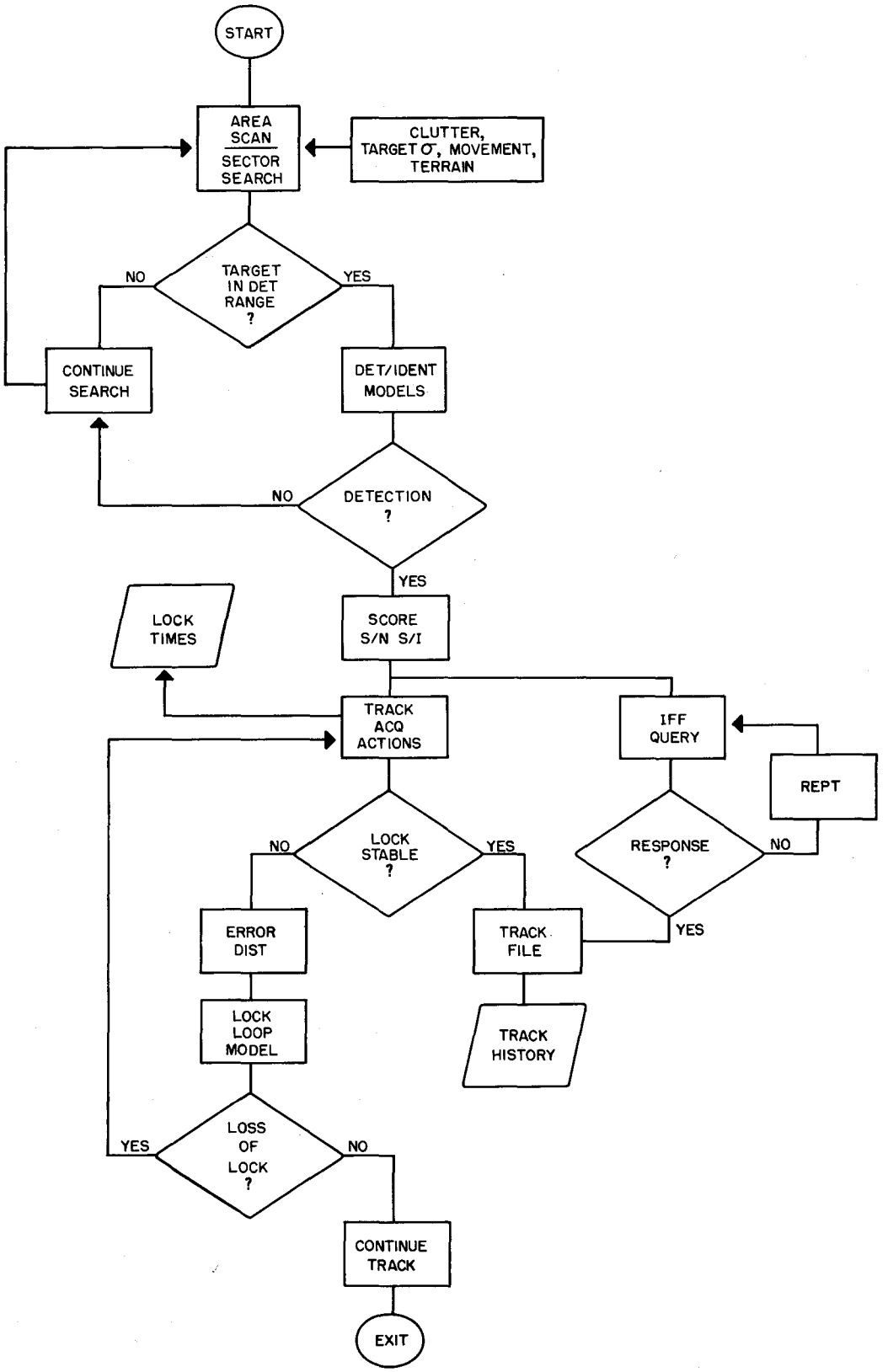

Figure 7.3. General radar operations diagram.

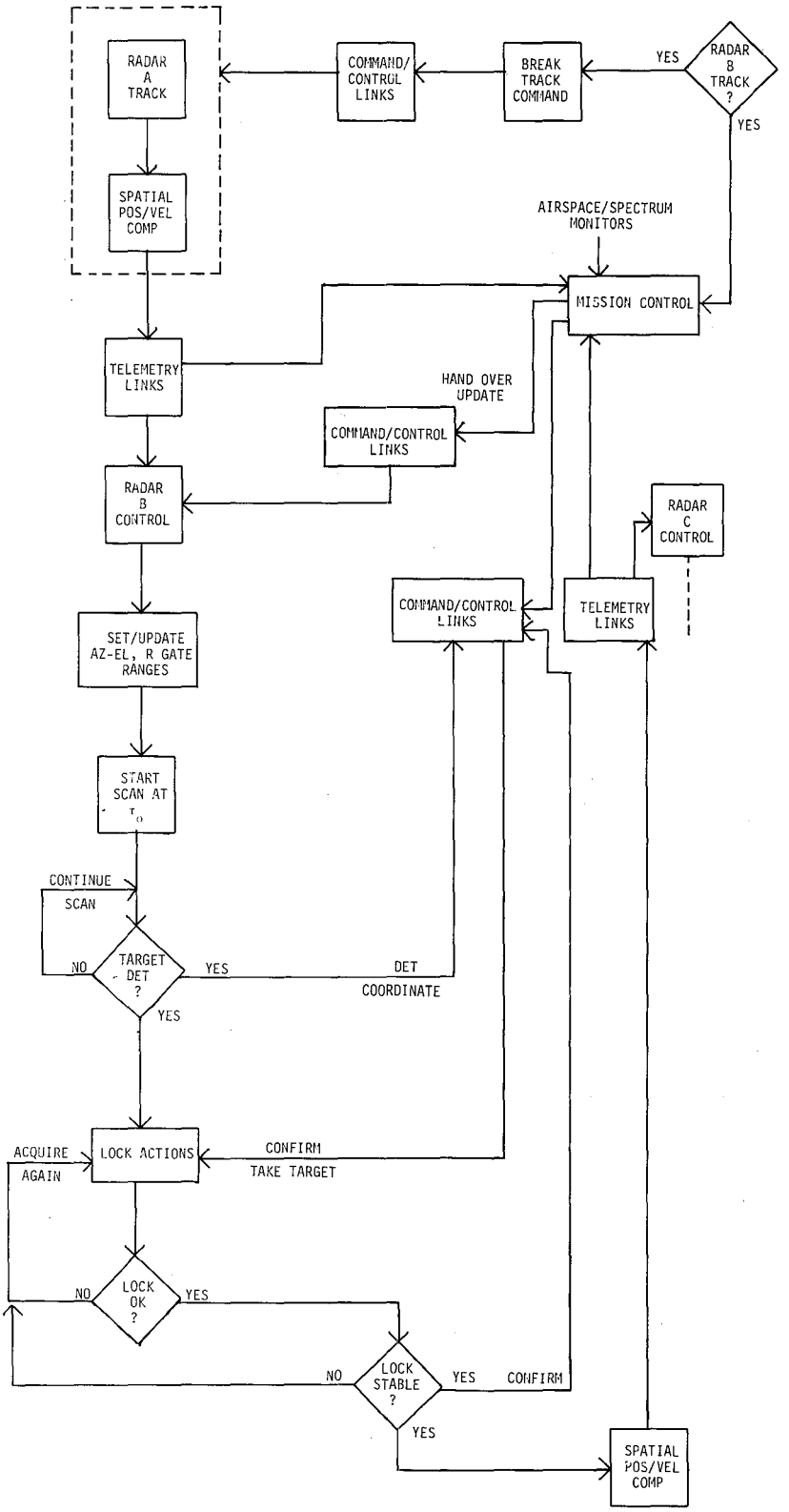

Figure 7.4. General range radar hand over procedure.

Commercial communications operate in the 2 GHz bands and 6 GHz bands. These include systems operated by the Union Pacific and Santa Fe railroads and the State of California backbone network. These systems operate 200 and 400 channel FDM analog equipments. Other networks using 50-200 channel configurations serve utility and pipeline control and utility operations. The commercial equipments use paraboloid and high gain yagi antennas, since the flexibility in signal sources required for military test range operations is not required. Commercial microwave systems are generally single frequency, fixed-path configurations where military microwave systems at the effected ranges generally require moving antennas and multiple frequency use.

The upper hierarchy of the operations specifications for a communications network used for utility service on pipeline command/control is presented in Figure 7.5. Critical events are indicated, correlating to the performance criteria listed in Section 7.5.

7.2 Military Signal Monitor Receiver Evaluation

This class of equipment includes the various configurations of tactical receivers used for signal search, classification and identification, posture assessment, and EMC management. The system can include 2 or 4 antennas, a frequency scanning receiver, analog or digital modulation component separation, and a computer for signal files, comparison logic, alarm and display operation, and EMC control. Performance effects include the receiver and computer areas. The susceptibility scoring criteria are listed below:

RECEIVER

a. Intermodulation related signal density.
b. Modulation component separation errors.
c. Signal direction of arrival errors.

COMPUTER

a. Signal density saturation.
b. False alarm - control action probabilities.
c. Signal identification errors.
d. Signal processing delays.

This receiver system (typical of a threat warning system) is generally employed with operational test and evaluation exercises, therefore being important in the capabilities of range facilities located near the China Lake range. The evaluation of this equipment demonstrated the level of degradation to be experienced by such operations. During war games that are designed to simulate various real tactical

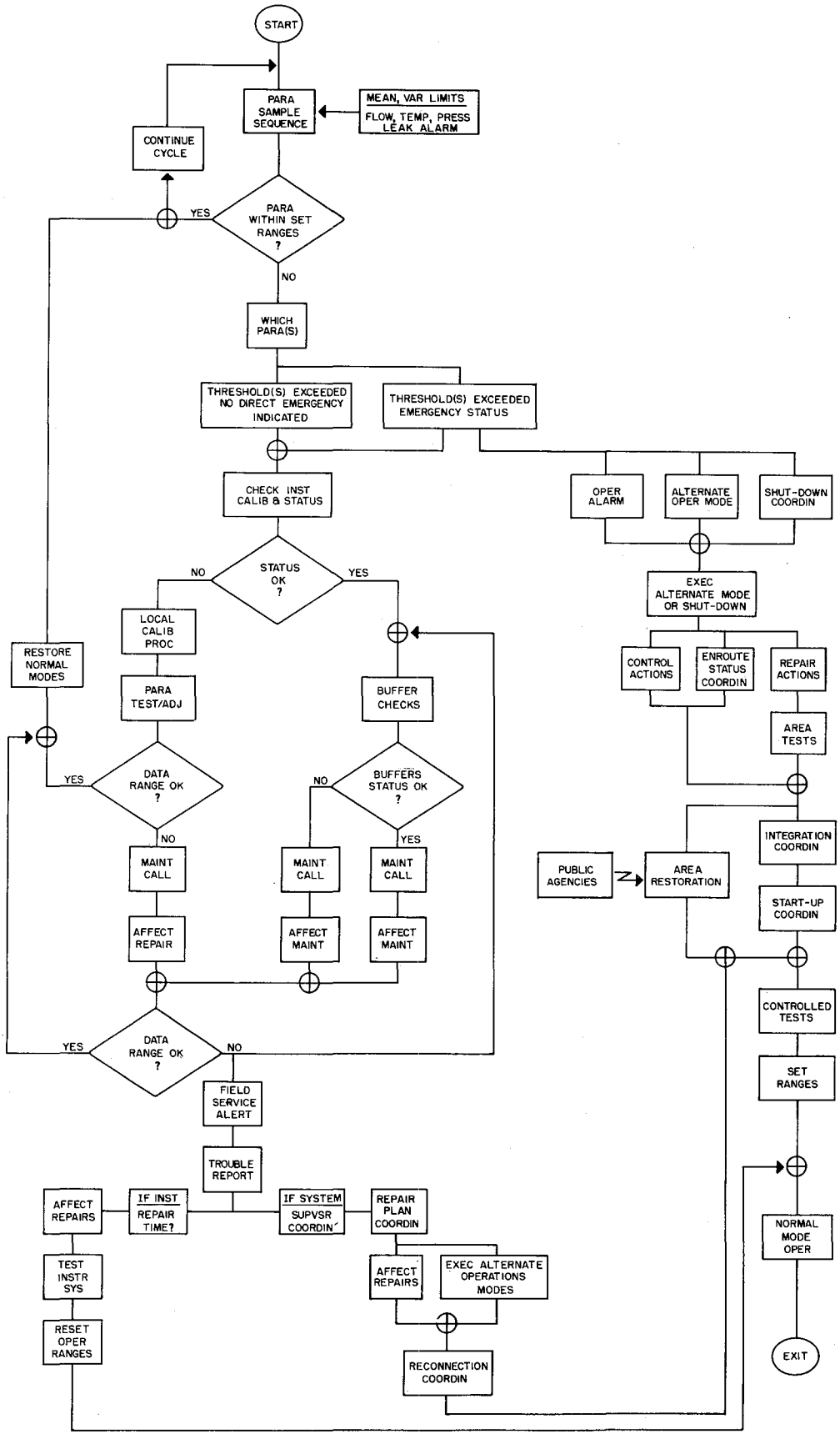

Figure 7.5. General network C^3 operations support modes.

situations for design of battlefield strategy, erroneous information or wrong procedural specifications could result if systems were modified for SPS mitigation purposes biasing the interaction between this type of receiver and the signal environment. These operational ranges include control and monitoring facilities that require functional authenticity and would be very sensitive to the electromagnetic environment. Simulation of tactical situations in parts of the world where no SPS exists could not be achievable if biasing by SPS occurred in these systems.

7.3 Sensor Evaluation

Scanning sensors such as TV cameras were tested by subjecting them to simulated SPS field intensities that would be encountered outside a rectenna exclusion area. The sensors were checked under these conditions for increased video noise and scan jitter and decreased spatial resolution and dynamic range. These parameters are related to requirements for security monitors and target tracking. The specific scoring criteria have different weighting in these applications; software feature extraction as employed for security systems exploits spatial image characteristics and movement (frame-to-frame comparison) detection.

Sensor testing for the Mojave evaluation included 525-line video cameras, 1000-line video cameras, forward-looking infrared (FLIR) detectors, and small mosaic staring visual spectra and IR sensors. The basic methodology is diagrammed in Figure 7.6, indicating the target image application, EM energy coupling, and measurements. Bar targets were used for the visual scanners, the maximum resolution being 2000 lines/inch. The IR bar targets included reflectance (2 to 6η) elements with a 1000 lines/inch resolution, and differential temperature bar targets (800 lines/inch) for the thermal sensors (8 to 13η).

Radiation coupling involved a horn radiator illuminating the sensor and control system directly into the optical aperture, $\pm 30°$ off the optical axis, at the sides of the camera and electronic control units, and directly into nonmetallic and cable entry areas of the outer casing. The most sensitive areas by a 2 to 10 dB range were the nonmetallic casing (openings > 4 inches in one dimension) and the optical aperture. Generally, semiconductor detectors exhibit a susceptibility of 1 to 3 dB greater than vidicon or plumbicon tubes; this is approximately the same noise increase as large aperture photomultiplier tubes.

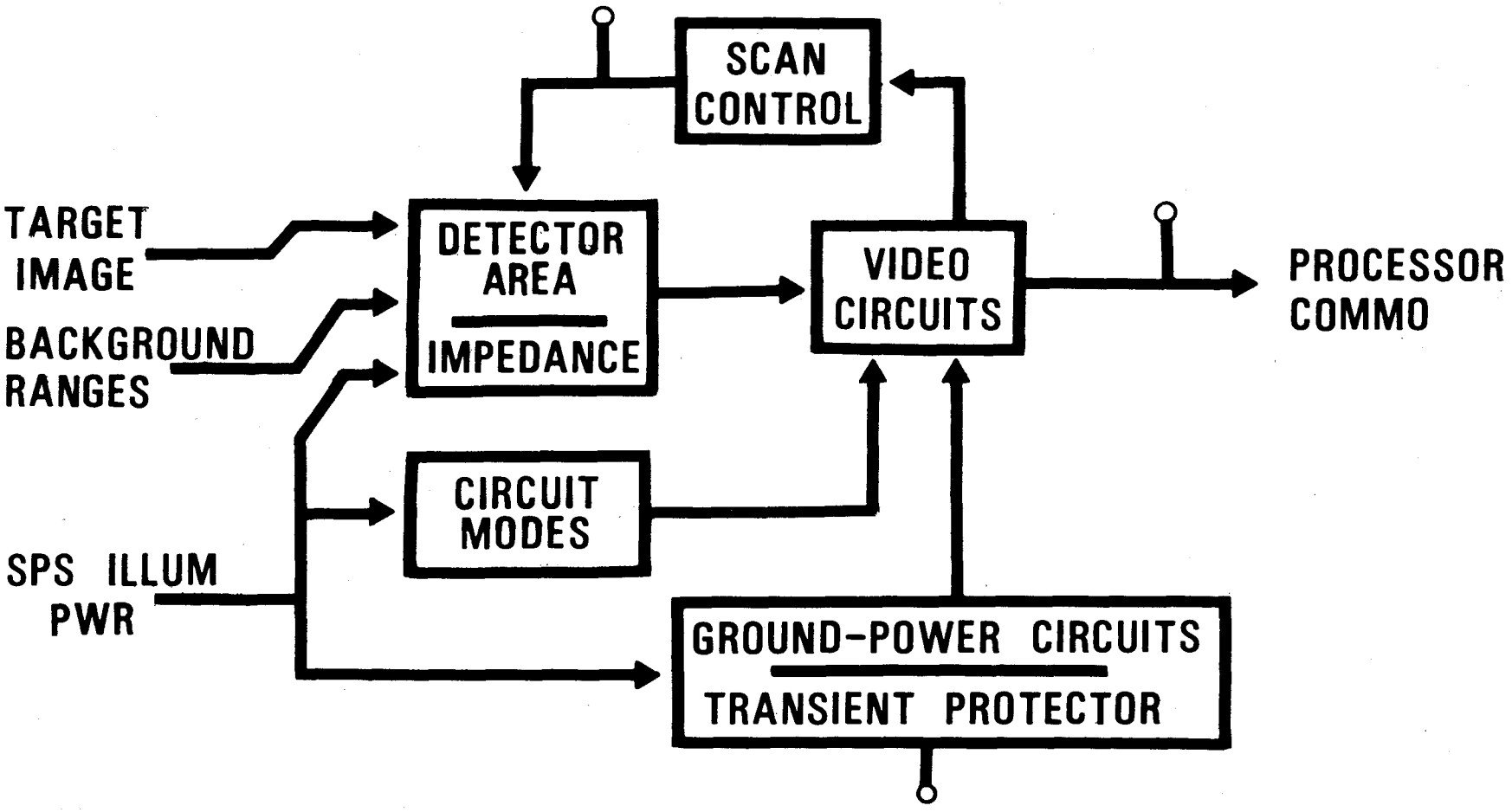

Figure 7.6. Image sensor-signal and energy coupling.

The scoring criteria for the various sensor categories are listed below:

SCANNING SENSORS

a. Video noise amplitude.
b. Video dynamic range.
c. Image resolution.
d. Scan jitter.

STARING SENSORS

a. Signal channel noise amplitude.
b. Minimum detectable target.
c. Dynamic range.

7.4 Computer/Processor Evaluation

The susceptibility testing for mini/micro computers included direct radiation of modules and noise conductivity tests for quality and power ground connections. Distributed processors and integrated systems were tested. The basic functional elements are indicated in Figure 7.7.

The performance criteria are listed below:

INTEGRATED PROCESSOR

a. I/O channel noise.
b. I/O register noise and transfer errors.
c. Control and clock bus noise.

DISTRIBUTED PROCESSOR

a. Module I/O channel noise.
b. Module control and clock bus noise, pulse jitter.
c. Module - module transfer errors.
d. Arithmetic module throughout errors.

The rapid evolution of microprocessors in hardware and software guided the test specifications. Measurement methods and module-system extrapolation relative to application routine impacts (e.g., contention delays, looping probabilities) were of concern as inputs to the EMC Guidelines document for reasonable cost diagnostics procedures.

Processors tested include 4, 16, and 32 bit formats, as used and proposed for central/distributed computation and file manipulation, mobile terminal, and data logging applications. Military processors included weapon data computation, sensor control, and file processing functions.

Commercial and military modules varied significantly in shielding integrity and grounding practice. These areas are major contributors to the susceptibility of these systems to interference problems (e.g., analog-digital conversion noise, input-output register control pulse jitter, control gate uncertainties in memory and transfer functions).

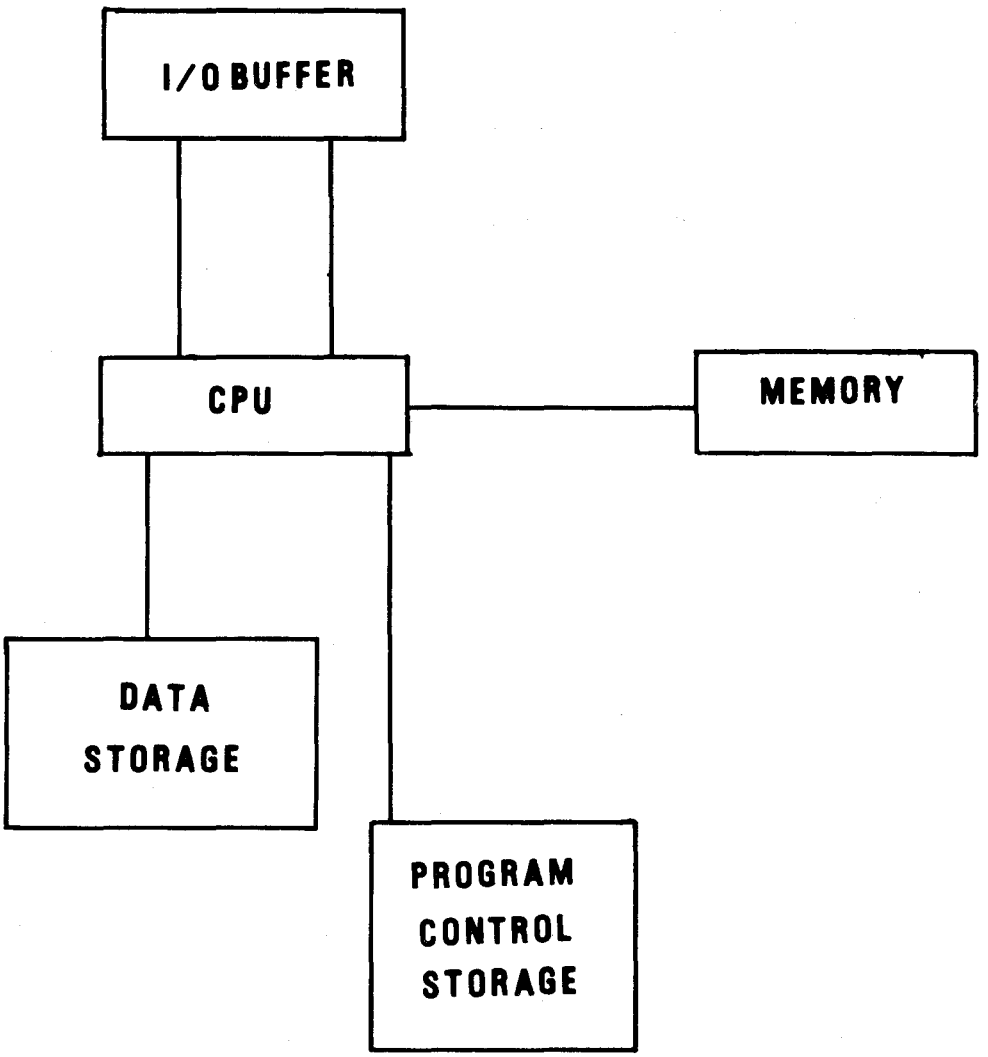

Figure 7.7. Mini-micro processor configuration.

7.5 System Functional Degradation

The functional degradation of radars, telecommunications systems, sensors, mini/microcomputers, and the threat warning receiver are tabulated in Table 7.1. Detailed analysis showing how the degradation estimates were derived will be published in a separate report on SPS effects on a large number of EM and electronic systems. Ranges of effects are indicated to accommodate the variations in operational modes and SPS power densities where a particular equipment may be deployed over a large area (e.g., range radars, command/control and telemetry, railroad, and California State microwave systems).

Table 7.1

SPS Induced System Degradation

Function	Characteristic Effects
Instrumentation Radar (Military Test Ranges)	a. Cooperative target acquisition range: -(8-20%) b. Skin target acquisition range: -(13-28%) c. Cooperative target track error: +(15-40%) d. Skin target track error: +(22-65%) e. Loss of track loop lock (skin mode) probability increase: +(10-40%)
Command/Control and Telemetry Communications (Military Test Ranges)	a. Signal acquisition threshold: +(5-20%) b. Data error: +(5-28%) c. Sync loss probability: +(3-25%)
Tactical Signal Identification - Analysis System	a. False alarm probability outside mission zone: +(3-25%) b. False alarm probability within mission zone: +(18-60%) c. Receiver noise threshold: +(5-40%) d. Signal processing time: +(45-115%) e. Software overload probability increase: +(2-26%)
IR Scanner (Tactical System)	a. Video noise threshold: +(2-26%) b. Target detection identification error probability: -(5-33%)
Utility and Pipeline Command/Control/Telemetry Communications	a. Signal acquisition threshold: +(5-15%) b. Data error: +(10-30%) c. Link noise: +(5-20%)
Image Intensifiers	a. Video noise level: +(10-45%) b. Standard target detection/identification range: -(5-30%) c. Multiple target spatial resolution: -(2-60%)
Non-Federal Government Communications	a. Channel noise: +(5-15%) b. Data error: +(8-35%)

As mentioned previously, the elements of performance degradation cited for the functional systems represent an average overall operating mode and geographic range. For example, instrumentation radar systems detection and tracking performance includes operation over a full hemisphere coverage and the range of cross-section magnitudes for military target vehicles (e.g., tactical fighter and reconnaissance aircraft, target drones, and transponder variations) during a track period. Track score variations include low elevation angle modes, where the accuracy degradation and loss of lock probabilities expand by greater margins because of propagation factors. On-axis radar configurations are also represented since this mode will probably be increasingly employed for these test range applications. The track error scores include normal smoothing, prediction filtering, and coordinate computations in real-time and with postmission processing software.

The communications system degradation cited includes single channel and frequency and time multiplexed units operated by the military test ranges, the State of California, local county and municipal governments, and resource control and service industries.

8. OPERATIONAL IMPACT AREAS

The performance changes cited must be translated into compromises in a supported operation or service to assess an impact on public service or safety. These operational impacts are described in decision trees relating functional characteristics to action events and resulting service capabilities or safety risks. These relationships are particularly evident in relating radar and associated communications system performance to the air space monitoring mission and transportation safety through the air traffic control process.

There are a number of fixed microwave multi-user communication systems which traverse the Mojave area. These include the State of California backbone network which handles communications involving law enforcement, forest fires, natural resource management, natural disasters (flood, earthquakes, etc.), and other state administrative information and data; national communication trunks providing common carrier services such as Bell Telephone, GTE, and MCI microwave links; railroad microwave systems which carry train information and data. For these systems a direct relationship to safety is evident only during local emergencies such as forest fire, train wreck, tornado, etc. Even in such cases, the situation is not immediately managed through these systems but through local police, fire

departments, emergency disaster teams, etc., closest to the problem area. Any potential functional degradation caused by SPS in these types of fixed position microwave systems can be mitigated by fairly straightforward techniques.

A detailed analysis of operational impacts of SPS illumination on military systems surrounding this particular Mojave site is not warranted. Functional modifications of operational equipments at these test and evaluation facilities represent an unaccceptable risk in the training and doctrinal study missions as explained in more detail in 8.1 and 8.2 below. These considerations led to the decision that this particular hypothetical Mojave site would not be acceptable. (See Section 9 for recommendations.)

8.1 Range Instrumentation

This equipment category includes the numerous radars and associated TV camera equipment employed for spatial position and orientation tracking at China Lake, Edwards AFB, and Echo Range. These radars provide the basic tracking of airborne vehicles operating to test equipment effectiveness, including interaction in simulated engagement with surface defense units. The radars, identified in the previous section, include units that are slaved through command/control networks for target acquisition and "hand-over" to cover large-area flight operations. Data telemetry from these radars includes rectangular spatial position coordinates, rectangular coordinate velocity data, and signal characteristics that are employed for diagnostics. These instrumentation radars must satisfy an accuracy requirement of 1.5 to 5 meters in position for elevation angles above 15°, and 5 to 15 meters for the lower elevation angle tracking modes. Where increased accuracy in lower angles is required, the video records can be employed with the radar range and coordinate data to improve resolution. Previous accuracy requirements are based upon the use in the processing cycle of normal smoothing and predictive filtering processes.

As indicated previously, the primary effects of the SPS power densities predicted for China Lake, Edwards AFB, and Echo Range cause increased noise in the predetection components of the receivers, reductions in target acquisitions range, and increased data error during track. Considering the deployment of radars on these facilities, an increased gap in coverage would result because of the reduced detection range. These comments are also applicable to the TV cameras at Edwards AFB, primarily, as noted previously, because the problem for the TV detector would be reduced by a factor of 2 to 3 for particular cameras procured by China Lake.

This tracking instrumentation must operate over an entire hemisphere to effectively support the operational exercises at these facilities. The SPS effect would be reduced if elevation were limited to approximately 50°, but this represents an impossible compromise for the military exercises.

The representative instrumentation time line for a normal test involving one or more aircraft includes premission calibration and coordinate slaving, acquisition command cycles, track confirmation, track, event tagging, and hand-over events. This indicates the general chronology of the radar and video equipment acquisition and track cycles. The interaction with command/control networks is indicated in relation to the initiation of different modes. Typical effects of the SPS induced degradation include uncertainties and delays in acquisition and additional communications activity necessary from the command/control network for instrumentation control, slaving data-flow control, and hand-over. Increased gaps in radar coverage and data errors are assured.

The primary effects, as noted in the previous section, for the data networks at these facilities relate to signal acquisition and data error rates. These translate into operational problems in greatly increased activity through the data network because of synchronization and error effects.

A combination of error problems and an increase in the net activity at the various test ranges would reduce the capability to support simultaneous missions. This is particularly important in engagement evaluation where numerous remote-controlled facilities may be involved and delays in communication events would represent an unacceptable experimental bias. Since such engagements generally involve event-related activities, for example, aircraft evasive maneuvers, or electronic countermeasure initiations in response to identification of a specific received signal mode or the onset of a transmission on a particular signal frequency, the validity of most multiple vehicle experiments would be unacceptable. These comments are qualitatively correct on the basis of the deployment of command/control and instrumentation equipments, the magnitude of the SPS interference, and previous histories at other test ranges where an EMC situation caused similar compromises in instrumentation and network performance.

8.2 Operational Systems

The China Lake area ranges generally evaluate weapons systems performance and limited operational engagements. The latter includes, for example, delivering of ordinance and the collection of surveillance data in the presence of a simulated hostile environment. These tests, therefore, are very dependent upon

the EM support systems such as radars, command/control, and sensors. Considering the frequency range of military operational equipments employed for tactical aircraft and the aperture of electro-optical devices supporting tactical missions, the SPS power densities would eliminate effective testing except for very short ranges of deployment. Modifications to tactical equipment to accommodate the SPS are not possible because of the compromises and biases in relation to realism in event sequences and the correlation between operational and functional events such as the interaction between electronic instrumentation and combat and support equipment operations.

A representative surveillance and weapons delivery time line includes regress, route command/control, reference point identification, entry maneuvers with radar and EW scanner operations, penetration command/control, target entry communications, sensor search and track, weapons control or surveillance search operations, and regress communications. For multiple aircraft, for example, the previously cited command/control network activity increases represent severe constraints in the number of vehicles that can be supported and significantly increases the potential for missed events and thus destroys mission credibility.

Operational test facilities in the area have the principle purpose of evaluating proposed EM penetration support equipment and procedures and providing operational training and doctrine testing for tactical air force penetration against hostile air defense systems. Replicated environments are generated that interact with penetrating EW systems and control maneuvers and equipment operation for testing and training purposes. Critical events for EM systems include signal detection, signal source recognition and mode analysis, and counteractive interaction events. The capability to detect, identify, and classify specific signal characteristics and to locate emitters is fundamental to the self-protection or standoff support for aircraft penetrating protected zones. These include air-air and air-ground EM system interactions.

The facility includes operational monitoring capabilities to score all events relating to the survivability of surface elements and aircraft. Test facility operations would be impeded in range of coverage and event recognition because of the SPS power densities, thus presenting bias and error in doctrinal and procedural decisions and improper event histories for training exercises.

9. CONCLUSIONS AND RECOMMENDATONS

This preliminary assessment of SPS microwave emissions on "victim" systems as given here demonstrates the operational degradation that would occur to

electronic systems in the SPS generated environment within approximately 100 km of the hypothetical site. This Mojave site evaluation shows a wide range of performance degradation, particularly in those systems operated by the military. The basic functional and operational impacts of SPS are of such magnitude that in many instances they represent unacceptable or impossible compromises and biases to sensitive test and evaluation exercises performed by the involved facilities.

As mentioned previously, the evaluation of the hypothetical Mojave rectenna site provided impact data to NASA, contributed to site selection and evaluation criteria, and allowed a limited exercise of the data retrieval and analysis procedures that were required for the EMC analysis of other candidate CONUS sites. This Mojave site originally considered allowed a reasonable rectenna site because of the isolation from areas of even modest population density. At this site, the majority of the severe impact interference problems concerned military operation, the degraded systems being integral components of complex Development and Operational Test and Evaluation programs. These military programs require the degree of isolation afforded by the Mojave region.

Based on the operational system degradations near the Mojave site and the inability to establish mitigating strategies without unacceptable operational compromise, a second hypothetical site north and east of the original site was reviewed by ITS. A cursory look at the "victim" systems surrounding the new site indicates different functional classes which lend themselves to mitigating strategies. There were only 400 operational systems, mainly civilian and FAA links. Modifications to most of these systems could be accomplished to produce compatibility in the SPS generated environment.

The functional degradation of military, nondefense government, and commercial systems in the Mojave area is basically characteristic of the effects that will be encountered in other CONUS areas as far as the generic systems of Table 7.1 are concerned. Operational impacts, and therefore the associated economic impact, will vary by area because of differing uses, configurations, and priority functions the degraded equipment support.

The Mojave area lends itself well to resiting because of the large expanse of open, flat terrain. The development of new sites in most geographic areas would be more difficult, if not impossible, due to population density, terrain features, "victim" system density, etc.

As given by FCC and NTIA printouts of EM systems operating in northern and eastern CONUS regions, generally there will be a smaller concentration of

military-nondefense equipment in proximity to hypothetical areas which could possibly support a rectenna site than the hypothetical Mojave site under study here. These regions, however, include major transportation and commercial communications facilities and relatively large populations of susceptible computers, sensors, and control complexes associated with power generation and distribution, mass transportation, and industrial control facilities. Because of the higher population and business densities compared to the Mojave desert area, the total number of affected systems in the various operational categories on page 56 will be larger. However, this means more systems that may need mitigation techniques within a given area, not necessarily more complex techniques.

A valid demonstration of rectenna site EMC analysis and impact evaluation has been developed. This has been shown to be fundamental in supporting site selections, in helping to determine system performance impacts, and in helping to develop mitigating strategies for victim systems.

10. REFERENCES

Ahmed, I. Y., and L. J. Auchterlonie (1976), Microwave measurements on dust, using an open resonator, Electronic Letters, 12, No. 17, pp. 445-446.

Battan, L. J. (1973), Radar observation of the atmosphere, (University of Chicago Press, Chicago), IL, p. 259.

Battelle Pacific Northwest Laboratories (1978), Initial assessment, electromagnetic compatibility aspects of the proposed microwave systems, PNL-2482.

Bean, B. R., and E. J. Dutton (1968), Radio Meteorology, (Dover Publications Inc., New York, NY), pp. 269-308.

Bean, B. R., E. J. Dutton, and B. D. Warner (1970), Weather effects on radar, Radar Handbook, (McGraw-Hill Book Co., Inc., M. I. Skolnick, Editor, New York, NY), pp. 24-22.

Blake, Lamont V. (1966), Antennas, (John Wiley & Sons, New York, NY), p. 174.

Boeing Aerospace Company, Missiles and Space Group - Space Division (1976), Initial Technical environmental and economic evaluation of space solar power concepts, Vol. I: Summary, and Vol. II: Detailed Report, (NAS TMX74389 9jsc-11568).

Born, M., and E. Wolf (1959), Principles of Optics, (Pergamon Press, New York, NY), pp. 391-400.

Brooks, C. E. P., and N. Carruthers (1953), Handbook of Statistics in Meteorology, (Her Majesty's Stationery Office, London, U.K.), pp. 86-87.

Crane, R. K. (1970), A comparison between monostatic and bistatic scattering from rain and thin turbulent layers, Lincoln Laboratory, Massachusetts Institute of Technology, Lexington, MA, Tech. Note 1970-29.

Dickinson, R. M. (1977), Satellite power system microwave subsystem impacts and benefits, California Institute of Technology, Jet Propulsion Lab., JPL 900-800.

Dutton, E. J. (1967), Estimation of radio ray attenuation in corrective rainfalls, J. of App. Meteorology 6, No. 4, pp. 662-668.

Dutton, E. J. (1977), Precipitation variability in the U.S.A. for microwave terrestrial system design, OT Report 77-134, (Defense Documentation Center Access No. ADA049041).

Eberhardt, E. W. (1977), Candidate locations for SPS rectifying antennas, NSAS-TM-78146.

El-Fandy, M. G. (1953), On the physics of dusty atmospheres, Quart. J. Royal Meteorological Soc. 79, No. 340, pp. 284-287.

FCC Rules and Regulation, Vol. II, August 1976; Vol. III, August 1976; Vol. IV, March 1977; Vol. V, December 1974; Vol. VII, March 1974; Vol. III, March 1971; Vol. IX, June 1976; and Vol. XI, August 1976. Federal Comm. Commission, Washington, D.C., Superintendent of Documents, (U.S. Government Printing Office, Washington, D.C. 20401).

Fraser, R. S. (1959), Scattering properties of atmospheric aerosols, Department of Meteorology, University of California at Los Angeles, (NTIS Access No. 233-288).

General Secretariat of the International Telecommunication Union (1978), Radio Regulations of the ITU, Vol. I - Radio Regulations, Additional Radio Regulations, Vol. II - Appendicies to the Radio Regulations, Resolutions and Recommendations, Geneva, ISBN: 92-62-00181-5.

Harvey, A. F. (1963), Microwave Engineering, (Academic Press, John Wright & Sons, Ltd., London, U.K.), p. 253.

Idso, S. B., R. S. Ingram, and J. M. Pritchard (1972), An american haboob, American Meteorological Society Bulletin 6, No. 10, pp. 930-935.

Janes, H. B., J. T. Collins, and F. K. Steele (1978), A preliminary catalog of programs and data for 10-100 GHz radio system predictions, OT Report 78-141, (NTIS Access No. PB280774/AS).

Liebe, H. J., and G. G. Gimmestad (1977), Calculation of clear air refractivity, Radio Sci. 13, No. 2, pp. 245-251.

Ma, M. T. (1974), Theory and Application of Antenna Arrays, (Wiley-Intrascience, New York).

Oliver, F. W. (1945), Dust-storms in Egypt and their relation to the war period, as noted in Maryut, 1939-1945, Geographical J. 106, pp. 26-49.

U.S. Department of Energy (1978), Satellite power system (SPS) concept development and evaluation program plan, July 1977 - August 1980, DOE/ET-0034.

U. S. Department of Energy (1978), Satellite power system (SPS) concept development and evaluation program - work breakdown structure, FY 1978 - 1980.

USNWS, World-wide airfield summaries, Vol. VII, Part 1 (1969), U.S. Naval Weather Service, (NTIS Access No. 688-472).

White, D. (1972), A Handbook Series on Electromagnetic Interference and Compatibility, Vol. 5, EMI Predictions and Analysis Techniques, (Library of Congress Catalog Card No. 72-138-444).

FORM NTIA-29
(4-80)

U.S. DEPARTMENT OF COMMERCE
NAT'L TELECOMMUNICATIONS AND INFORMATION ADMINISTRATION

BIBLIOGRAPHIC DATA SHEET

	1. PUBLICATION NO. NTIA Report 81-76	2. Gov't Accession No.	3. Recipient's Accession No.

4. TITLE AND SUBTITLE
Electromagnetic Compatibility Analysis For A Satellite Power System Receiving Site in the Mojave Desert.

5. Publication Date
June 1981

6. Performing Organization Code

7. AUTHOR(S)
E. L. Morrison, W. B. Grant, and E. J. Dutton

9. Project/Task/Work Unit No.

8. PERFORMING ORGANIZATION NAME AND ADDRESS
National Telecommunications & Information Admin.
Institute for Telecommunication Sciences
325 Broadway
Boulder, CO 80303

10. Contract/Grant No.

11. Sponsoring Organization Name and Address
U.S. Department of Energy
Washington, C.C. 20545

12. Type of Report and Period Covered

13.

14. SUPPLEMENTARY NOTES

15. ABSTRACT *(A 200-word or less factual summary of most significant information. If document includes a significant bibliography or literature survey, mention it here.)*

The Department of Energy (DOE), along with the National Aeronautics and Space Administration (NASA), has been evaluating the Satellite Power System (SPS) as a source of baseline electrical power. The objective of the SPS program is to develop an initial understanding of the technical feasibility, the economic practicality, and the social and environmental acceptability of the SPS concept. One of the potential problems identified early in the concept analysis was the electromagnetic compatibility (EMC) of an SPS with existing and planned electromagnetic and electronic systems. A preliminary study has been conducted to show the EMC problems for an initial candidate receiving antenna (rectenna) site in the Mojave Desert of California. A methodology has been developed and demonstrated for rectenna site EMC analysis and impact evaluation. For the particular site chosen,

(continued next page)

16. Key Words *(Alphabetical order, separated by semicolons)*

17. AVAILABILITY STATEMENT ☒ UNLIMITED. ☐ FOR OFFICIAL DISTRIBUTION.	18. Security Class. *(This report)* UNCLASSIFIED	20. Number of pages 78
	19. Security Class. *(This page)* UNCLASSIFIED	21. Price:

☆ U.S. GOVERNMENT PRINTING OFFICE: 1981 — 780-658/425 Region No. 8

15. ABSTRACT (Cont.)

the majority of the severe impact interference problems concerned military operations. The systems degraded by SPS off-site microwave beam components were integral systems and subsystems of complex Development and Operational Test and Evaluation programs. Based on the operational system degradations near the Mojave site and the inability to establish mitigating strategies without unacceptable operational compromise, a second site north and east of the original was proposed.